the lowest symmetry, from 21 to 15). In particular, they reduce the number of independent moduli in isotropic and hexagonal systems from two to one, setting the Lamé coefficients λ and μ equal to each other. In our analytical calculations, we will, however, treat λ and μ as independent. The Cauchy limit is easily obtained by setting $\lambda = \mu$. However, as we have seen [Eq. (2.43)]p, random δK leads to corrections to Eq. (3.17) when relaxation relative to the affine limit are allowed. These corrections violate the Cauchy relations.

IV. MARGINALLY COORDINATED LATTICES AND THE MAXWELL-CALLADINE THEOREM

References:

Lubensky, T. C., C. L. Kane, Xiaoming Mao, A. Souslov, and Kai Sun. “Phonons and Elasticity in Critically Coordinated Lattices.” Reports on progress in physics. Physical Society (Great Britain) 78, no. 7 (2015-Jul 2015): 073901.

Mao, X. M., and T. C. Lubensky. ”Maxwell Lattices and Topological Mechanics.” In Annual Review of Condensed Matter Physics, Vol 9, edited by S. Sachdev and M. C. Marchetti. Annual Review of Condensed Matter Physics, 413-33, 2018.

A. Introduction

So far, these lectures have focused on continuum elastic media or lattices that are mechanically stable. In what follows, we will study lattices that are on the verge of mechanical stability. Such lattices include familiar ones like the square and kagome lattices with nearest neighbor (NN) springs, Penrose tilings and quasicrystals with NN springs, and packed spheres at the jamming transitions.

In a remarkable 1864 paper , James Clerk Maxwell undertook the first systematic study of the mechanical stability of frames consisting of points, which we will refer to as *sites*, with connections, which we will usually refer to as *bonds*, between them as a model for such real-world structures as the Warren Truss (patented in 1848) shown in Fig. 5. He defined a “stiff” frame as one in which “the distance between two points cannot be altered without changing the length of one or more connections”. He showed that a stiff frame containing

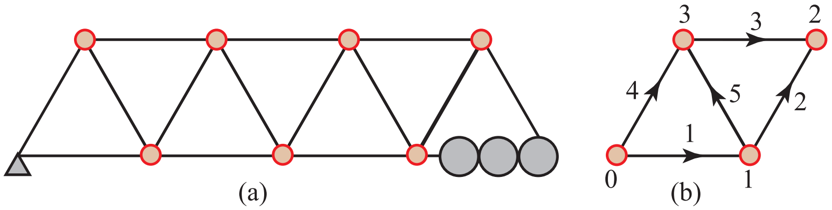

FIG. 5. (a) The Warren Truss, which is composed of equilateral triangles with $N = 9$ sites and $N_B = 15$ connections, so that $2N - N_B = 3$. The lower left site (indicated by the small triangle) is fixed with respect to the earth, and the lower right site is constrained to move only horizontally along a track with wheels. These constraints reduce the number of free degrees of freedom of the sites by 3 to $N_{\text{free}} = 2N - 3 = 15 = N_B$. This frame obeys a definition of isostatic that it have no zero modes or states of self stress that is more restrictive than $d = 2z$. (b) A reduced version of the isostatic Warren Truss indicating conventions for labeling sites and bonds. The arrows indicate bond directions following the convention described in section IV C, Eqs. (4.12) to (4.15).

N sites in d dimensions requires

$$N_B = dN - w(d) \tag{4.1}$$

connections, where $w(d) = d(d+1)/2$ is the number of rigid translations and rotations under free boundary conditions. Under periodic boundary conditions, which Maxwell did not consider, $w(d) = d$. This relation, often referred to as *Maxwell's rule*, can be reexpressed as a critical coordination number ($z \equiv 2N_B/N$),

$$z_c^N = 2d - 2\frac{w(d)}{N}. \tag{4.2}$$

If $z < z_c^N$, the system is not stiff, and if $z > z_c^N$, it is. As we shall discuss in more detail in the next section, Maxwell's rule for the stability of frames requires modification . Nevertheless, it provides a useful and universally used benchmark for the analysis of the stability of frames. We will refer to free frames, i.e., ones under free boundary conditions, satisfying Maxwell's rule as *Maxwell frames*. It is fairly common practice to use the term *isostatic* for frames satisfying Maxwell's rule. Though isostatic frames do satisfy Maxwell's rule, they have more restrictive properties, discussed in Fig. 5.

Our principal interest here is in frames whose sites can be collected into identical contiguous unit cells whose origins lie on a Bravais lattice and which fill some region of space. We will refer to these frames as *lattices* and if they are subjected to periodic (free) boundary

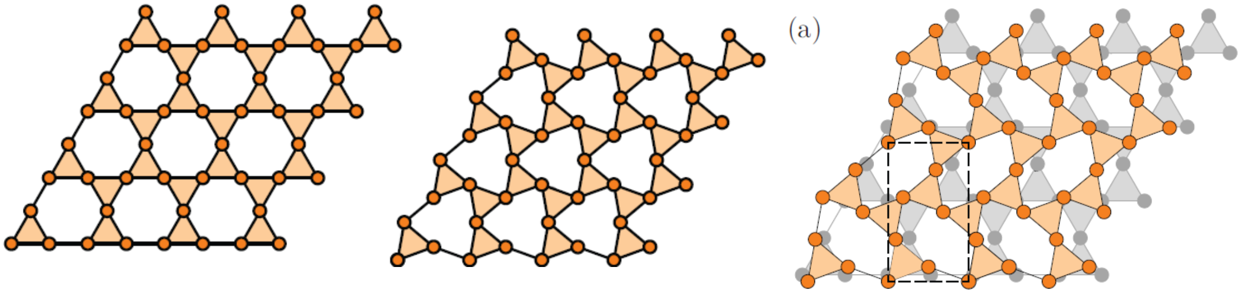

FIG. 6. Examples of periodic Maxwell lattices based on the (a) kagome lattice; (b) twiosted kagome lattice; (c) larger unit-cell twisted kagome lattice.

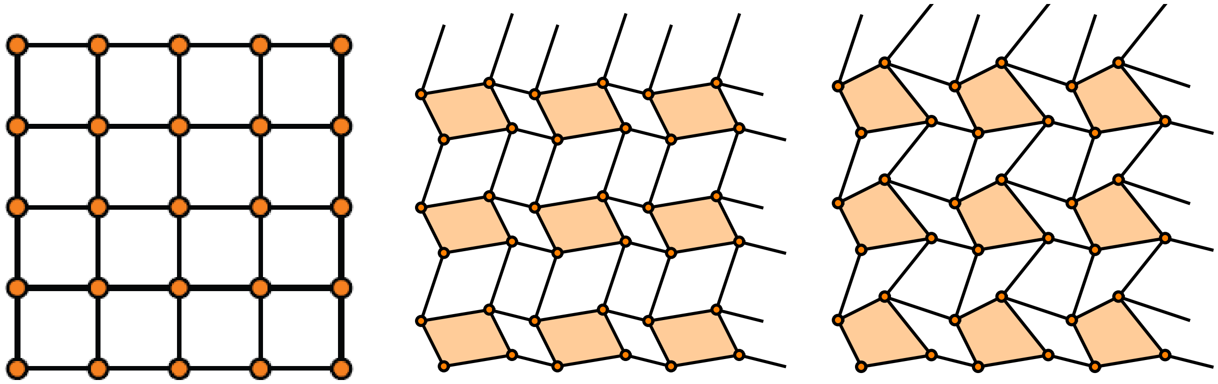

FIG. 7. Examples of periodic Maxwell lattices based on the (a) square lattice; (b) and (c) distorted square lattices with four-cite unit cells.

conditions as periodic (free) lattices. Any frame, even those that are not lattices, e.g., whose sites are randomly distributed, can also be subjected to periodic (free) boundary conditions in which case we will refer to them as periodic (free) frames. For reasons that we will justify more fully later, we will use the term *periodic Maxwell frame (lattice)* for periodic frames (lattices) with average coordination number $z_c = 2d = z_c^\infty$ rather than z_c^N. Free frames can be liberated from periodic ones by cutting of order $N^{(d-1)/d}$ bonds.

Maxwell's analysis applies to frames with an arbitrary number of sites and bonds. In addition to being a workhorse of the structural engineering community , it has seen extensive use (though not always with attribution to Maxwell) in physics, materials science, and mathematics. It is a critical component of the theory of structural glasses , rigidity percolation , framework silicates like β-cristobalite , jamming of packed spheres , biopolymer networks , and of some theories of protein folding . Rigidity percolation and jamming

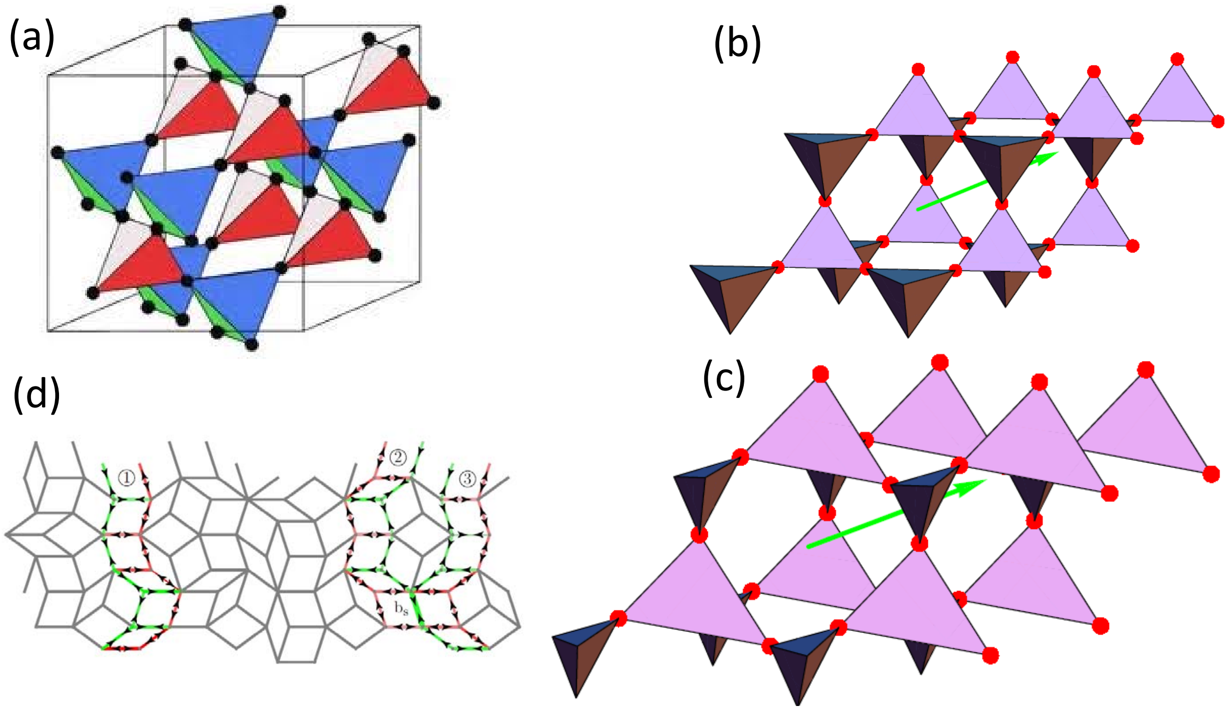

FIG. 8. Examples of 3D periodic Maxwell lattices based (a) pyrochlore lattice, (b) and (c) distorted phrochlore lattices; (d) quasicrystalline Penrose tiling.

generally involve central forces only, and the Maxwell relation and its generalization can be applied to these problems directly. Structural glasses and biopolymer networks have bending forces that require a modification of the Maxwell rules, and we will not make much contact with them in what follows.

B. The Maxwell Rule and States of Self Stress

Each site in d-dimensions has d independent translational degrees of freedom, and in the absence of constraints on point motion, a collection of N points without connections has $N_{\text{free}} = dN$ zero-frequency displacement modes, which we will refer to as *zero modes*. In the presence of constraints, N_{free} will be less that dN. Each connection reduces the number of zero modes by one. Thus if there are N_B connections and no constraints, there are

$$N_0 = dN - N_B \tag{4.3}$$

zero modes. Of these, $w(d)$ are the trivial ones associated with rigid translations and rotations. Any other zero modes involve internal displacements of the sites and are generally

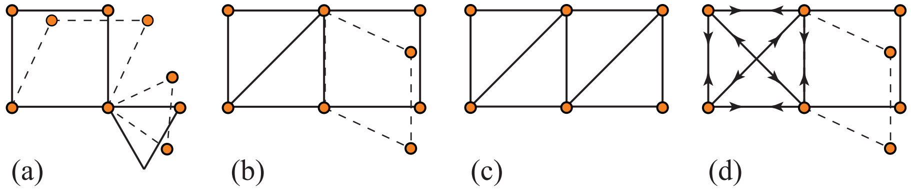

FIG. 9. (a) to (c) Frames satisfying the Maxwell rule. (a) has 6 sites, 7 bonds, 5 zero modes, and two mechanisms indicated by the dotted bonds. (b) has 6 sites, 8 bonds, 4 zero modes, and one mechanism. (c) and (d) are constructed from (b) by adding an additional diagonal bond. (c) satisfies the Maxwell rule with only the three trivial zero modes. (d) has 4 zero modes and one state of self stress indicated by the arrows on the bonds in the left square.

called *mechanisms* in the engineering literature and *floppy modes* in the physics literature . Equation (4.3) reexpressed in terms of the number of mechanisms M is

$$M = dN - N_B - w(d). \tag{4.4}$$

We will refer to Eqs. (4.3) and (4.4) as the *Maxwell count.* A frame is stiff if it has no mechanisms. Setting $M = 0$ yields the Maxwell rule [Eqs. (4.1)]. Figure 9(a) depicts a simple frame that obeys Maxwell's count. It consists $N = 6$ sites and $N_B = 7$ bonds, and it has $N_0 = 2 \times 6 - 7 = 5$ zero modes and $M = N_B = 5 - 3 = 2$ mechanisms.

The simple Maxwell rule does not apply to all frames . Consider the two-square frame with $N = 6$ sites and $N_B = 8$ bonds shown in Fig. 9(b). It has one mechanism as expected from the Maxwell count. If an extra bond is added, Maxwell's rule would say that the frame is stiff with no mechanisms. The extra bond, however, can be placed as a diagonal in the right square [Fig. 9(c)] or as an extra diagonal in the left square [Fig.!9(d)]. In the first case, there are no mechanisms, and Maxwell's rule applies. In the second case, however, the mechanism present before the extra bond was added remains, and the Maxwell count is violated. But the left square with crossed diagonal bonds has an extra *redundant* bond not needed for its rigidity. It also has a new and interesting property: the outer bonds of the square can be placed under tension (compression) and the inner diagonal bonds under compression (tension) such that the net force on all sites is zero. This is a *state of self stress*, which, because of its repeated use in this review, we will usually abbreviate as SSS. This theme can clearly be repeated with each added bond either decreasing the number of zero modes or increasing the number of states of self stress to yield the modified Maxwell count :

$$N_0 = dN - N_B + N_S \qquad \text{or} \qquad N_0 - N_S = dN - N_B, \tag{4.5}$$

where N_S is the number of SSSs. This is an *index theorem* , which we will derive in section IV C, relating mode and self-stress count to geometric properties of the lattice. We will refer to it simply as the Index theorem .

Two types of mechanisms can be distinguished: “finite” ones in which finite-amplitude displacements of sites stretch no bonds and “infinitesimal” ones in which bond lengths do not change to first order in the magnitude of displacements but do so to second (or higher) order. The Index theorem , as we shall show below, follows from the assumption of a linear relation between site displacements and bond lengths, and it treats all displacements as infinitesimal, i.e., it counts both finite and infinitesimal mechanisms but does not identify which is which. Figures 10(a)-(b) show how a finite mechanism can be converted into two infinitesimal mechanisms and one SSS. A configuration of self-stress that is particularly important for the current study is any straight line of bonds under periodic boundary conditions, which we will refer to as straight *filaments*, as shown in figures 10(c)-(d). Changing the straight filament to a zigzagged one removes this state of self stress. On the other hand the “zigzaging” periodic ladder configuration shown in Fig. 10(e) has one SSS, rather than the two that a straight ladder would have. Tensions alternate in sign from bond to bond in this SSS, a property, which will be important in what follows, that prevents it from having any zero wave-number component.

A system in which there are neither any mechanisms ($M = 0$) nor any states of self-stress ($N_S = 0$) is *isostatic* . A finite isostatic system necessarily satisfies the Maxwell relation $z = z_c^N$, but a system with $z = z_c^N$ can have any number of mechanisms provided it is equal to the number of SSSsa. The distinction between satisfying the Maxwell rule and being isostatic is often lost in the literature, and it is common practice to refer to any system that satisfies Maxwell’s rule as isostatic. In this review, we will keep the distinction, referring to any free frame satisfying Maxwell’s rule as a Maxwell frame, reserving the term isostatic for those free Maxwell frames satisfying $M = N_S = 0$. The extension of this definition to periodic frames presents some problems . Since the term isostatic has become so prevalent, we propose in that section a definition of this term that is in the spirit of the definition for free frames and consistent with common usage for periodic frames.

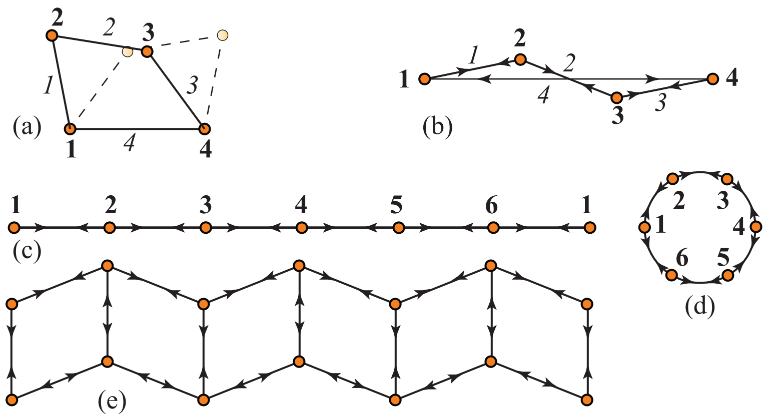

FIG. 10. States of self stress: (a) A frame with four sites (**1-4**) and four bonds (italic *1*, *2*, *3*, and *4*) with 4 zero modes and one finite mechanism (dashed lines); (b) A frame in which the length of bond *4* is equal to the sum of the lengths of bonds 1 to 3. Now there is a SSS in which bond *4* is under compression (tension) and the other three are under tension (compression). Both sites **2** and **3** can undergo infinitesimal displacements without changing the length of any bonds, and there are two infinitesimal mechanisms. (c) A line of parallel bonds forming a sample-traversing filament under periodic boundary conditions as depicted in (d). The forces on all sites are zero if all of the bonds are under equal tension or compression, and there is one SSS. (e) A zigzag ladder under periodic boundary conditions with one SSS.

C. Equilibrium and Compatibility Matrices

In the absence of external forces, the equilibrium force at each site in a frame is determined by the tensions in the bonds it shares with other sites. This is true whether or not the site is in mechanical equilibrium; if the force at a site is nonzero, the mass at that site will accelerate according to Newton's laws. If forces at sites arising from bond tensions are nonzero, they can be balanced by external loads to create an equilibrium situation in which the total force on each site is zero. Clearly, in mechanical equilibrium, the external loads are the negative of the forces at each site arising from bond tensions.

For central forces, the tension in a bond is parallel to the bond. Thus its direction is specified by bond orientation, but its magnitude and sign can vary. Let F be a vector in the dN-dimensional space, V_{F}, of the d components of force at each site on the lattice exerted by tensions in the bonds that terminate on it, and let T be a vector in the N_B-dimensional space, V_{T}, of the of the bond tensions, which are scalars of either sign. External loads at sites are represented by the dN-dimensional vector L. In equilibrium when sites do not accelerate (or move if there is external friction), $\mathsf{L} = -\mathsf{F}$. Since the relation between forces and tensions is linear, there is a $dN \times N_B$ dimensional matrix Q (with dN rows and N_B columns), called the *equilibrium* matrix, that maps V_{T} to V_{F}:

$$\mathsf{Q}\,\mathsf{T} = -\mathsf{F} = \mathsf{L}, \tag{4.6}$$

where the final relation only applies in static situations.

The null space or kernel of Q, $\ker(\mathsf{Q})$ of dimension $\text{nullity}(\mathsf{Q})$, is the set of all vectors mapped to the zero vector. Any vector in the null space of Q represents a state of self stress because it corresponds to tensions on a set of bonds for which the forces on all sites are zero. Thus $\text{nullity}(\mathsf{Q})$ is equal to the number of SSSs N_S. Vectors T not mapped into the null space of Q are in the *orthogonal complement*, $OC(\mathsf{Q})$, of $\ker(\mathsf{Q})$. The dimension of $OC(\mathsf{Q})$ is equal the to the rank of Q. The rank-nullity theorem of linear algebra relates the rank and nullity of a matrix to its column dimension:

$$\text{rank}(\mathsf{Q}) + \text{nullity}(\mathsf{Q}) = \text{rank}(\mathsf{Q}) + N_S = N_B. \tag{4.7}$$

Elongation of bonds are determined by the displacements of the sites to which they are attached. The elongations of individual bonds are necessarily parallel to bond vectors for central forces. Let U be a vector in the dN-dimensional space, V_{U}, of site displacements and E be a vector in the N_B-dimensional space, V_{E}, of bond elongations. The $N_B \times dN$-dimensional compatibility matrix C maps V_{U} to V_{E}:

$$\mathsf{C}\,\mathsf{U} = \mathsf{E}. \tag{4.8}$$

The null space of C is the set of displacements U that do not change the length of bonds, i.e., the set of zero modes of the system; thus, $\text{nullity}(\mathsf{C}) = N_0$. The rank-nullity theorem applied to C yields

$$\text{rank}(\mathsf{C}) + \text{nullity}(\mathsf{C}) = \text{rank}(\mathsf{C}) + N_0 = dN. \tag{4.9}$$

The equilibrium and compatibility matrices are not independent: they are matrix transposes of each other. To see this, we can calculate the work done under infinitesimal distortions of the system in the presence of sites forces (and thus necessarily tensions in the bonds) in two ways: First the work W_L done by external loads in displacing sites and second the work

W_T done by bond tensions in stretching bonds. The two calculations must yield the same result:

$$W_L = \mathsf{L}^T\mathsf{U} = \mathsf{T}^T\mathsf{Q}^T\mathsf{U} = W_T = \mathsf{T}^T\mathsf{E} = \mathsf{T}^T\mathsf{C}\mathsf{U}, \tag{4.10}$$

where the superscript T refers to the transpose of a matrix. Since this relation is valid for all U (even U in the null space of C) it must be that $\mathsf{C} = \mathsf{Q}^T$. The rank of a matrix is equal to the rank of its transpose, $\text{rank}(\mathsf{Q}) = \text{rank}(\mathsf{C})$, and subtracting Eq. (4.7) from Eq. (4.9) yields the Index theorem of Eq. (4.5). The equilibrium and compatibility matrices have proven useful in many contexts, and we mention only one in which frames with spring lengths that do not correspond to the length of the bonds they occupy are constructed from frames in which they do .

To construct Q and C for a particular frame, it is necessary to have explicit representations for the vectors U, E, T, and F. A frame consists of N sites labeled $s = 1, ..., N$ at equilibrium positions $\mathbf{R}(s)$ connected by N_B bonds labeled $\beta = 1, ..., N_B$. Under frame distortions, site positions change to

$$\mathbf{X}(s) = \mathbf{R}(s) + \mathbf{u}(s), \tag{4.11}$$

where $\mathbf{u}(s)$ with components $u_i(s)$, $i = 1, ..., d$, is the displacement vector at site s. The force at site s is $\mathbf{f}(s) = (f_1(s), ...f_d(s))$, and the dN-dimensional displacement and force vectors are, respectively, $\mathsf{U} = (\mathbf{u}_1, ..., \mathbf{u}_N)$ and $\mathsf{F} = (\mathbf{f}_1, ..., \mathbf{f}_N)$.

Each bond $\beta = [s_\beta, s'_\beta]$ connects a pair of sites s_β and s'_β, whose separation in the equilibrium frame is the vector

$$\boldsymbol{b}(\beta) \equiv \boldsymbol{b}([s_\beta, s'_\beta]) = \mathbf{R}(s'_\beta) - \mathbf{R}(s_\beta) \equiv b_\beta \hat{\boldsymbol{b}}_\beta, \tag{4.12}$$

from s_β to s'_β, where b_β is the length of bond β and $\hat{\boldsymbol{b}}_\beta$ is the unit vector along bond β. The arrows in Fig. 5(b) show an arbitrarily chosen choice of directions of vectors $\hat{\boldsymbol{b}}_\beta$ for bonds in a simple frame. Other choices will lead to different equations relating forces to tensions but will not affect the physical tensions in the frame. Let the tension in bond β be t_β, and associate with that bond a vector tension,

$$\boldsymbol{t}_\beta = t_\beta \hat{\boldsymbol{b}}_\beta. \tag{4.13}$$

With this convention, the force exerted on sites s_β and s'_β by bond $[s_\beta, s'_\beta]$ are, respectively, $\boldsymbol{t}_\beta$ and $-\boldsymbol{t}_\beta$, or, equivalently, the force on a site s from a bond β that it shares with another site is $\boldsymbol{t}_\beta$ if $\hat{\boldsymbol{b}}_\beta$ points away from the site and $-\boldsymbol{t}_\beta$ if it points toward the site. With these definitions, we can construct the compatibility matrix from the the bond elongation relations,

$$e_\beta = \hat{\boldsymbol{b}}_\beta \cdot (\mathbf{u}(s'_\beta) - \mathbf{u}(s_\beta)), \tag{4.14}$$

and the equilibrium matrix from the site force equations,

$$\mathbf{f}(s) = \sum_{\beta=1}^{z_s} \operatorname{sign}(\beta)\boldsymbol{t}_\beta, \tag{4.15}$$

where z_s is the number of bonds site s shares with its neighbors and $\operatorname{sign}(\beta) = +1(-1)$ if the arrow of bond β points away from (toward) site s.

It is instructive to carry out explicit calculations of Q and C for a simple frame. We consider the frame shown in Fig. 5(b) with $N = 4$, $N_B = 5$ and $2N - N_B = 3$, the number of modes of rigid translation and rotation. This frame has no floppy modes and no state of self stress, and it is isostatic. The figure labels sites $(s = 0, ..., 3)$, bonds $(\beta = 1, ..., 5)$, and bond directions. The five displacement-elongation equations are

$$\begin{aligned}
&e_1 = \hat{\boldsymbol{b}}_1 \cdot (\mathbf{u}_1 - \mathbf{u}_0) &\quad& e_2 = \hat{\boldsymbol{b}}_2 \cdot (\mathbf{u}_2 - \mathbf{u}_1) &\quad& e_3 = \hat{\boldsymbol{b}}_3 \cdot (\mathbf{u}_2 - \mathbf{u}_3)\\
&e_4 = \hat{\boldsymbol{b}}_4 \cdot (\mathbf{u}_3 - \mathbf{u}_0) && e_5 = \hat{\boldsymbol{b}}_5 \cdot (\mathbf{u}_3 - \mathbf{u}_1), &&
\end{aligned} \tag{4.16}$$

and the four vector force equations are

$$\begin{aligned}
&\mathbf{f}_0 = \boldsymbol{t}_1 + \boldsymbol{t}_4 &\quad& \mathbf{f}_1 = -\boldsymbol{t}_1 + \boldsymbol{t}_2 + \boldsymbol{t}_5\\
&\mathbf{f}_2 = -\boldsymbol{t}_2 - \boldsymbol{t}_3 && \mathbf{f}_3 = \boldsymbol{t}_3 - \boldsymbol{t}_4 - \boldsymbol{t}_5.
\end{aligned} \tag{4.17}$$

The 8×5 compatibility and 5×8 equilibrium matrices are easily constructed from equations (4.16) and (4.17). If, however, we are interested only in internal deformations of the frame and not its uniform translations and rotations, we can apply three constraints to the motion, most easily by pinning site 0 so that $\mathbf{u}_0 = 0$ and placing site 1 on a horizontal rail as shown in Fig. 5(a) to fix $u_{1,y} = 0$ so that $N_{\text{free}} = 5$. We also allow $\mathbf{f}_0$ and $f_{1,x}$ to take on whatever values needed to satisfy the constraints, so they do not enter into our equations. This leaves us with a 5×5 compatibility matrix,

$$\mathsf{C} = \begin{pmatrix} 1 & 0 & 0 & 0 & 0 \\ -\frac{1}{2} & \frac{1}{2} & \frac{\sqrt{3}}{2} & 0 & 0 \\ 0 & 1 & 0 & -1 & 0 \\ 0 & 0 & 0 & \frac{1}{2} & \frac{\sqrt{3}}{2} \\ \frac{1}{2} & 0 & 0 & -\frac{1}{2} & \frac{\sqrt{3}}{2} \end{pmatrix}, \tag{4.18}$$

mapping $\mathsf{U} = (u_{1,x}, u_{2,x}, u_{2y}, u_{3,x}, u_{3,y})$ to $\mathsf{E} = (e_1, e_2, e_3, e_4, e_5)$. The equilibrium matrix, mapping $\mathsf{T} = (t_1, t_2, t_3, t_4, t_5)$ to $\mathsf{L} = -\mathsf{F} = -(f_{1,y}, f_{2,x}, f_{2,y}, f_{3,x}, f_{3,y})$ constructed from Eq. (4.17), is trivially equal to C^T. Both Q and C are square invertible matrices: their nullspaces are empty, both $N_0 = 0$ and $M = 0$, and the system is isostatic as required. Thus, the tensions on the bonds are uniquely determined by the forces on the sites and vice versa: the frame is *statically determinate*. And the elongations of the bonds are uniquely determined by the site displacements and vice versa: the frame is *kinematically determinate*. Thus, an alternative, and perhaps preferable, definition of an isostatic frame is that it be both statically and kinematically determinate. Another way of dealing with the trivial zero modes is to introduce "reaction forces" to yield 8×8 matrices Q and C.

D. Periodic Lattices with a Basis

A general lattice has N_c unit cells consisting of n sites and n_b bonds so that the total number of sites and bonds are, respectively, $N = N_c n$ an $N_B = N_c n_b$. The Bravais lattice vectors $\boldsymbol{R}_\ell$, where $\ell = (l_1, \cdots l_d)$ with each l_i an integer, are linear combinations of the primitive translation vectors $\boldsymbol{a}_j$, $j = 1, \cdots d$:

$$\boldsymbol{R}_\ell = \sum_j^d l_j \boldsymbol{a}_j. \tag{4.19}$$

The positions of sites and bonds in cell ℓ in the undistorted lattice with a basis are

$$\begin{aligned} \boldsymbol{R}_{\ell,\mu} &= \boldsymbol{R}_\ell + \boldsymbol{r}_\mu, \qquad \mu = 1, \cdots, n \\ \boldsymbol{R}_{\ell,\beta} &= \boldsymbol{R}_\ell + \boldsymbol{r}_\beta, \qquad \beta = 1, \cdots, n_b, \end{aligned} \tag{4.20}$$

where $\boldsymbol{r}_\mu$ and $\boldsymbol{r}_\beta$ are, respectively the positions of the sites and bonds relative to the origin of the unit cell. The positions of lattice sites in a distorted lattice are

$$\boldsymbol{X}_{\ell,\mu} = \boldsymbol{R}_{\ell,\mu} + \boldsymbol{u}_\mu(\ell), \tag{4.21}$$

where $\boldsymbol{u}_\mu(\ell)$ with Cartesian components $u_{\mu,i}(\ell) \equiv u_\sigma(\ell)$, where $\sigma = (\mu, i)$, is the displacement vector of site (ℓ, μ). The components of U are thus the dN displacements $u_\sigma(\ell)$. The Cartesian components $f_\sigma(\ell)$ of the force vector $\boldsymbol{f}_\mu(\ell)$ are the dN components of F. The N_B bond elongations $e_\beta(\ell)$ and bonds tensions $t_\beta(\ell)$ are the components of the of E, and T, respectively. Fourier transforms in periodic lattices are defined in the usual way in terms of wavenumbers $\mathbf{q}$ in the first Brillouin zone:

$$\boldsymbol{u}_\mu(\ell) = \frac{1}{N_c}\sum_{\boldsymbol{q}} e^{i\boldsymbol{q}\cdot(\boldsymbol{R}_\ell+\boldsymbol{r}_\mu)}\boldsymbol{u}_\mu(\boldsymbol{q}), \qquad \boldsymbol{u}_\mu(\boldsymbol{q}) = \sum_\ell e^{-i\boldsymbol{q}\cdot(\boldsymbol{R}_\ell+\boldsymbol{r}_\mu)}\boldsymbol{u}_\mu(\ell) \tag{4.22}$$

$$e_\beta(\ell) = \frac{1}{N_c}\sum_{\boldsymbol{q}} e^{i\boldsymbol{q}\cdot(\boldsymbol{R}_\ell+\boldsymbol{r}_\beta)}e_\beta(\boldsymbol{q}) \qquad e_\beta(\boldsymbol{q}) = \sum_\ell e^{-i\boldsymbol{q}\cdot(\boldsymbol{R}_\ell+\boldsymbol{r}_\beta)}e_\beta(\ell), \tag{4.23}$$

and similarly for $\boldsymbol{f}_\mu$, $\boldsymbol{t}_\beta$ and other site and bond variables. These quantities can also be defined without the site and bond basis vectors, $\boldsymbol{r}_\mu$ and $\boldsymbol{r}_\beta$, in the exponentials, and we will usually leave them out. They will, however, be of use in our discussion of topological states.

In periodic lattices, the equilibrium and compatibility matrices become bloc diagonal with blocks consisting of the Fourier transforms of these matrices. For example,

$$\mathbf{Q}_{\sigma\beta}(\boldsymbol{q}) = \sum_\ell e^{-i\boldsymbol{q}\cdot(\boldsymbol{R}_{\ell,\sigma}-\boldsymbol{R}_{0,\beta})}\mathbf{Q}_{\sigma\beta}(\ell,0). \tag{4.24}$$

Again, the basis vectors in the exponents are not required. The compatibility matrix is $\mathbf{C}(\mathbf{q}) = \mathbf{Q}^\dagger(\mathbf{q})$.

With these definitions, we can reexpress equations (4.6) and (4.8) as

$$\mathbf{Q}(\boldsymbol{q})\,\mathbf{t}\,(\boldsymbol{q}) = -\mathbf{f}(\boldsymbol{q}) \qquad \mathbf{C}\,(\boldsymbol{q})\,\mathbf{u}(\boldsymbol{q}) = \mathbf{e}(\mathbf{q}), \tag{4.25}$$

where the "bold roman" vectors are defined as $\mathbf{t}(\mathbf{q}) = (t_1(\mathbf{q}), ..., t_{n_b}(\mathbf{q}))$ and $\mathbf{u}(\mathbf{q}) = (\mathbf{u}_1(\mathbf{q}), ..., \mathbf{u}_n(\mathbf{q}))$ and similarly for $\mathbf{e}(\mathbf{q})$ and $\mathbf{f}(\mathbf{q})$, and $\mathbf{Q}(\mathbf{q})$ is the $dn \times n_b$ matrix with components $\boldsymbol{Q}_{\sigma\beta}(\mathbf{q})$. There is one equation for each of the N_c values of $\boldsymbol{q}$, giving us as many independent equations as Eq. (4.6) and Eq. (4.8). The Index theorem applies to these equations for each $\mathbf{q}$:

$$n_0(\mathbf{q}) - n_s(\mathbf{q}) = dn - n_b, \tag{4.26}$$

where $n_0(\mathbf{q}) = \text{nullity}(\mathbf{C})$ is the number of zero modes and $n_s(\mathbf{q}) = \text{nullity}(\mathbf{Q})$ is the number of states of self stress at wavevector $\mathbf{q}$. Of course, $N_0 = \sum_{\mathbf{q}} n_0(\mathbf{q})$ and $N_S = \sum_{\mathbf{q}} n_s(\mathbf{q})$.

In periodic Maxwell lattices, $dn = n_b$, and there are exactly as many zero modes as states of self stress at each $\mathbf{q}$. Under PBCs, there are always d zero modes that arise from translational invariance, and these are necessarily at $\mathbf{q} = 0$, implying that there are at least d SSSs at $\mathbf{q} = 0$. There may be more, but each additional SSS will require an additional zero mode, which is a $\mathbf{q} = 0$ mechanism. At nonzero $\mathbf{q}$, there is no general reason for zero modes to exist, but if they do, the are necessarily accompanied by SSSs. We will see that this is a common theme in our study of specific lattices: removing states of self stress eliminates zero modes and "gaps" the phonon spectrum.

E. The Dynamical Matrix

So far, we have only discussed tensions and stretches of bonds without specifying any relation among them. In our "ball-and-spring" frames, each bond β is occupied by a Hooke's law spring whose energy is half its spring constant k_b times the square of its elongation. Let k be the $N_B \times N_B$ diagonal matrix of spring constants, then the elastic energy of the lattice is

$$V_{\mathrm{el}} = \tfrac{1}{2}\mathsf{E}^T\mathsf{k}\mathsf{E} = \tfrac{1}{2}\mathsf{U}^T\mathsf{K}\mathsf{U}, \tag{4.27}$$

where

$$\mathsf{K} = \mathsf{Q}\mathsf{k}\mathsf{Q}^T = \mathsf{C}^T\mathsf{k}\mathsf{C} \tag{4.28}$$

is the $dN \times dN$ *stiffness* matrix. Normal-mode frequencies depend on mass as well as the stiffness matrix. The kinetic energy requires the introduction of a mass matrix M. We will restrict our attention of frames in which the mass at all lattice is equal to m, in which case $\mathsf{M} = m\,\mathsf{I}$, where I is the unit matrix, and the kinetic energy is

$$E_{\mathrm{kin}} = \tfrac{1}{2}m\dot{\mathsf{U}}^T\dot{\mathsf{U}}, \tag{4.29}$$

where $\dot{\mathsf{U}}$ is the velocity vector. Normal modes are then eigenvectors of the *dynamical* matrix:

$$\mathsf{D} = \tfrac{1}{m}\mathsf{K}. \tag{4.30}$$

The Lagrangian in the presence of eternal loads is thus

$$L = \tfrac{1}{2}m\dot{\mathsf{U}}^T\dot{\mathsf{U}} - V_{\mathrm{el}} - \mathsf{U}^T\mathsf{L}, \tag{4.31}$$

and the equation of motion is

$$m\ddot{\mathsf{U}} = -\frac{\partial V_{\mathrm{el}}}{\partial \mathsf{U}^T} + \mathsf{L} = -\mathsf{K}\mathsf{U} + \mathsf{L} = \mathsf{F} + \mathsf{L}, \tag{4.32}$$

which vanishes when the external load L is equal to minus the force $-\mathsf{F} = \mathsf{K}\mathsf{U} = \mathsf{Q}\mathsf{T}$ exerted by bond stretching. Note that the equilibrium matrix can be used to calculate F whether or not the system is in static equilibrium or not. On the other hand $\mathsf{L} = \mathsf{QT}$ only in equilibrium when there is no acceleration (assuming no friction forces).

Following Eq. (4.27), the potential energy in terms of a periodic harmonic lattice is

$$V_{\text{el}} = \frac{1}{2N_c} \sum_{\boldsymbol{q}} \mathbf{e}^{\dagger}(\boldsymbol{q})\, \mathbf{k}\, \mathbf{e}(\boldsymbol{q}) = \frac{1}{2N_c} \sum_{\boldsymbol{q}} \mathbf{u}^{\dagger}(\boldsymbol{q}) \mathbf{K}(\mathbf{q}) \mathbf{u}(\boldsymbol{q}), \tag{4.33}$$

where $\mathbf{k}$ is the $n_b \times n_b$ diagonal matrix of spring constants, and

$$\mathbf{K}(\mathbf{q}) = \mathbf{Q}(\boldsymbol{q})\, \mathbf{k}\, \mathbf{Q}^{\dagger}(\boldsymbol{q}) \equiv m\mathbf{D}(\mathbf{q}) \tag{4.34}$$

is the stiffness matrix. We will usually set $m = 1$ so that the stiffness matrix $\mathbf{K}$ and the dynamical matrix $\mathbf{D}$ are the same. In periodic systems, nearest-neighbor (NN), next-nearest neighbor (NNN), and further-neighbor bonds are well defined, and bond vectors can be expressed as the direct sum of NN and NNN components, e.g. $\mathbf{e} = \mathbf{e}_{NN} \oplus \mathbf{e}_{NNN}$, and elastic constant matrix and dynamical matrices can be decomposed into NN and NNN:

$$\mathbf{D}(\mathbf{q}) = \mathbf{D}_{NN}(\mathbf{q}) + \mathbf{D}_{NNN}(\mathbf{q}). \tag{4.35}$$

F. The Elastic limit

Calculations of the elastic tensor require some method of maintaining strain. The usual picture is that boundary sites of a finite frame are clamped to conform with Eq. (2.36). Since these sites are fixed, their displacements and the forces associated with them do not enter the calculation of Q and C. An alternative approach, which we implement, is to apply periodic boundary conditions (PBCs) to the frame, which may or may not be composed of repeated unit cells. In this approach, it is the boundaries of the periodic cell that satisfy Eq. (2.36).

As we have seen, if the positions of all sites, rather than just boundary sites, displace according to Eq. (2.36), the elastic distortion is *affine*. Under such distortions, the relative displacement of the sites associated with bond β is

$$\mathbf{u}(s'_\beta) - \mathbf{u}(s_\beta) = \boldsymbol{\eta}\, (\mathbf{R}(s'_\beta) - \mathbf{R}(s_\beta)) = \boldsymbol{\eta}\, \boldsymbol{b}_\beta, \tag{4.36}$$

and the affine stretch of bond β is

$$e_\beta^{\text{aff}} = \hat{\boldsymbol{b}}_\beta^T\, \boldsymbol{\eta}\, \boldsymbol{b}_\beta = \hat{b}_{\beta,i} u_{ij} b_{\beta,j}, \tag{4.37}$$

where we used the fact that $\hat{b}_{\beta,i} b_{\beta,j}$ is symmetric in i and j to convert $\boldsymbol{\eta}$ to $\boldsymbol{u}$ in the linearized limit. The affine elastic energy density is then

$$f_{\text{el}}^{\text{aff}} = \frac{1}{2V}\, \mathsf{E}_{\text{aff}}^T\, \mathsf{k}\, \mathsf{E}_{\text{aff}}, \tag{4.38}$$

where V is the volume and E_{aff} is the vector of affine elongations e_β^{aff}.

Affine response is the exception rather than the rule. Here we show how the fully relaxed, non-affine elastic energy can be derived from the properties of the equilibrium and compatibility matrices and affine elastic energy just derived. Our starting point is Eq. (4.27) for the stretch energy in terms of the N_B dimensional bond-elongation vector E, which we break up into an affine part E_{aff} with components given by Eq. (4.37) and a part $\mathsf{C}\mathsf{U} = \mathsf{Q}^T\mathsf{U}$ describing additional changes in spring lengths that relax in response to the macroscopic strain imposed by E_{aff}. Multiplying Q^T on the left by the decomposition of the unit $N_B \times N_B$-dimensional matrix $\delta^{N_B} = \mathsf{P}_r^Q + \mathsf{P}_s^Q$ decomposed into the the projection operators, P_r^Q and P_s^Q, onto oc(Q) and ker(Q), respectively, and on the right by the decomposition of the dN-dimensional unit matrix into projections operators P_r^C and P_s^C onto oc(C) and ker(C), respectively, Q^T leads to the decomposition $\mathsf{Q}^T = \mathsf{Q}_{rr}^T + \mathsf{Q}_{sr}^T + \mathsf{Q}_{rs}^T + \mathsf{Q}_{ss}^T$, where $\mathsf{Q}_{sr}^T = \mathsf{P}_s^Q \mathsf{Q}^T \mathsf{P}_r^C$, and so on. When Q^T multiplies any vector to its right, the components of that vector in ker(C) are annihilated, and only the components in oc(C) survive. Thus, $\mathsf{Q}^T\mathsf{U} = (\mathsf{Q}_{rr}^T + \mathsf{Q}_{sr}^T)\mathsf{U}_r$. When this quantity is multiplied on the left by any N_B-dimensional vector W, the term involving $\mathsf{Q}_{sr}^T\mathsf{U}_r$ vanishes because it is orthogonal to oc(Q) and it gives zero for any vector in ker(Q). Thus, in V_{el}, $\mathsf{Q}^T\mathsf{U}$ can be replaced by $\mathsf{Q}_{rr}^T\mathsf{U}_r$. Similarly, $\mathsf{U}^T\mathsf{Q}$ can be replaced by $\mathsf{U}_r^T\mathsf{Q}_{rr}$, and the elastic energy as a function of U and E_{aff} is

$$V f_{\text{el}} = \tfrac{1}{2}(\mathsf{E}_{\text{aff}}^T + \mathsf{U}_r^T\mathsf{Q}_{rr})\mathsf{k}(\mathsf{E}_{\text{aff}} + \mathsf{Q}_{rr}^T\mathsf{U}_r). \tag{4.39}$$

Minimizing over the $dN - N_0$ independent components of U_r (or U_r^T) yields

$$V\frac{\partial f_{\text{el}}}{\partial \mathsf{U}_r^T} = \mathsf{Q}_{rr}\mathsf{k}(\mathsf{E}_{\text{aff}} + \mathsf{Q}_{rr}^T\mathsf{U}_r) = 0 \tag{4.40}$$

or, because both Q_{rr} and k_{rr} are invertible,

$$\mathsf{E}_{\text{aff},r} + \mathsf{Q}_{rr}^T\mathsf{U}_r = -(\mathsf{k}_{rr})^{-1}\mathsf{k}_{rs}\mathsf{E}_{\text{aff},s} \tag{4.41}$$

and

$$V f_{\text{el}} = \tfrac{1}{2}\mathsf{E}_{\text{aff},s}^T(\mathsf{k}_{ss} - \mathsf{k}_{sr}(\mathsf{k}_{rr})^{-1}\mathsf{k}_{rs})\mathsf{E}_{\text{aff},s} = \tfrac{1}{2}\mathsf{E}_{\text{aff},s}^T[(\mathsf{k}^{-1})_{ss}]^{-1}\mathsf{E}_{\text{aff},s}, \tag{4.42}$$

where $(\mathsf{k}^{-1})_{ss}$ is the projection of k^{-1} onto the null space of Q. This is Eq. (4.44). The final relation can be derived as follows: Let p be the inverse of k and decompose the two matrices into their projections onto the range and nullspace of Q,

$$\mathsf{k} = \begin{pmatrix} \mathsf{k}_{ss} & \mathsf{k}_{sr} \\ \mathsf{k}_{rs} & \mathsf{k}_{rr} \end{pmatrix} \qquad \mathsf{p} = \begin{pmatrix} \mathsf{p}_{ss} & \mathsf{p}_{sr} \\ \mathsf{p}_{rs} & \mathsf{p}_{rr}. \end{pmatrix} \tag{4.43}$$

Then $\mathsf{k}\,\mathsf{p} = \mathsf{I}$ implies that $\mathsf{k}_{ss}\mathsf{p}_{ss} + \mathsf{k}_{sr}\mathsf{p}_{rs} = \mathsf{I}_{ss}$ and $\mathsf{k}_{rs}\mathsf{p}_{ss} + \mathsf{k}_{rr}\mathsf{p}_{rs} = 0$. Thus, $\mathsf{k}_{ss} + \mathsf{k}_{sr}\mathsf{p}_{rs}\mathsf{p}_{ss}^{-1} = \mathsf{p}_{ss}^{-1}$ and $\mathsf{k}_{rs} = -\mathsf{k}_{rr}\mathsf{p}_{rs}\mathsf{p}_{ss}^{-1}$, and finally $\mathsf{k}_{ss} - \mathsf{k}_{sr}\mathsf{k}_{rr}^{-1}\mathsf{k}_{rs} = \mathsf{p}_{ss}^{-1} = [(\mathsf{k}^{-1})_{ss}]^{-1}$ as required. Thus the relaxed elastic energy density becomes

$$f_{\text{el}} = \frac{1}{2V}\mathsf{E}^{T}_{\text{aff},s}[(\mathsf{k}^{-1})_{ss})]^{-1}\mathsf{E}_{\text{aff},s} \xrightarrow{\mathsf{k}\to k\,\mathsf{I}} \frac{k}{2V}\sum_{\alpha}(\mathsf{E}_{\text{aff}}\cdot\hat{\mathsf{t}}_{\alpha})^2 \tag{4.44}$$

where $\mathsf{E}_{\text{aff},s}$ and $(\mathsf{k}^{-1})_{ss}$ are the projections of E_{aff} and k^{-1} onto $\ker(\mathsf{Q})$, and $\hat{\mathsf{t}}_{\alpha}$ is the αth orthonormal basis vector of $\ker(\mathsf{Q})$. Thus, only the projections of the affine displacement vectors onto states of self-stress contribute to the elastic energy.

Equation (4.44) encodes a great deal of information.

- First, it shows that lattices cannot be elastically stable unless they have SSSs in the presence of conditions that constrain the macroscopic strain - a simple reflection of the fact that forces on each site must be zero once equilibrium is reached in the presence of imposed strains, which necessarily induce bond tension.

- Second, only those states of self-stress with a nonzero overlap with the affine bond elongations contribute to the elastic energy. These states necessarily traverse the sample, and they are *load-bearing.* The straight filament of 10(c) (wound to a circle - Fig. 10(d)), whose bonds all have the same sign of tension provides an example of a load-bearing state, whereas the zigzag state of Fig. 10(e) and the localized crossed square of Fig. 9(d) does not.

- Third, because it is a sum of squares of linear combinations of strain, it shows that there must be at least $a_d = d(d+1)/2$ load-bearing SSS to produce an elastically stable system with an elastic matrix with a_d positive eigenvalues.

G. Guest-Hutchinson Modes in Periodic Maxwell Lattices

We have just seen that the elastic energy consists of a sum of $n_s(\mathbf{q}=0)$ positive terms. In order for the system to be stable with respect to elastic distortions (but not necessarily to ones at finite wavenumber), all $d(d+1)/2$ eigenvalues of the Voigt matrix must be positive. Thus, $n_0(\mathbf{q}=0)$ must be greater than or equal to $d(d+1)/2$, i.e. 3 in two dimensions and 6 in three dimensions. In Maxwell lattices, $n_s(\mathbf{q}=0) = n_0(\mathbf{q}=0)$. So there must be at least $d(d+1)/2$ zero modes at $\mathbf{q}=0$. Translational invariance dictates that there must be d zero modes at $\mathbf{q}=0$, and in lattices with fully gapped phonon spectra, there are no more than this number. But $d < d(d+1)/2$ implying that fully gapped lattices in two-dimensions have 1, and ones in three-dimensions have 3 zero energy mode of elastic distortion, respectively. These are the Guest Hutchinson modes.

The Guest-Hutchinson modes are necessarily accompanied by zero-frequency modes to linear order of non-zero wavenumber. To see how this comes about, consider the two-dimensional case for simplicity. There is one Guest-Hutchinson mode with strains u_{xx}^{GH}, u_{yy}^{GH} and u_{xy}^{GH}. At non-zero wavenumber the strain becomes $(\partial_i u_j + \partial_j u_i)/2$ so that

$$u_{xx}^{GH} = iq_x u_x, \qquad u_{yy}^{GH} = iq_y u_y \qquad u_{xy}^{GH} = i(q_x u_y + q_y u_x)/2. \tag{4.45}$$

These equations can be solved for $\lambda = q_y/q_x$:

$$\lambda_{\pm} = \frac{u_{xy}^{GH} \pm \sqrt{-\det \underset{\sim}{\mathbf{u}}^{GH}}}{u_{xx}^{GH}}. \tag{4.46}$$

Thus if neither u_{xx} nor u_{yy} are zero, these zero modes fall into two classes, one with $\det \underset{\sim}{\mathbf{u}}^{GH} > 0$ and one with $\det \underset{\sim}{\mathbf{u}}^{GH} > 0$. In the first class, λ_+ and λ_- have positive and negative imaginary parts, respectively, that lead to decaying and growing decay lengths $\pm \mathrm{Im}\, q_y$. These correspond to surface zero modes on opposite edges of a strip cut along the x-axis of a Maxwell lattice under periodic boundary conditions. Because $\det \underset{\sim}{\mathbf{u}}^{GH}$ is independent of choice of coordinate system, all edges must have zero surface modes. When $\det \underset{\sim}{\mathbf{u}}^{GH}_{xx} < 0$, λ_+ and λ_- are both real, and the GH-associated q-dependent modes are bulk modes along lines $q_y = \lambda_{\pm} q_x$. In most cases (e.g., topological lattices based on the kagome lattice to be discussed), the global count from the Index Theorem rules out true zero modes along these lines. Inclusion of third-order terms in q in C leads to frequencies proportional to q^2 along these lines, and in addition to surface modes whose inverse penetration depths scale as q^2

rather than as q. The situation is somewhat more complicated when either u_{xx}^{GH} or u_{yy}^{GH} is zero or there are more than one GH-mode.

V. KAGOME LATTICES

References

Kane, C. L., and T. C. Lubensky. "Topological Boundary Modes in Isostatic Lattices." Nature Physics 10, no. 1 (Jan 2014): 39-45.

Lubensky, T. C., C. L. Kane, Xiaoming Mao, A. Souslov, and Kai Sun. "Phonons and Elasticity in Critically Coordinated Lattices." Reports on progress in physics. Physical Society (Great Britain) 78, no. 7 (2015-Jul 2015): 073901.

A. The Kagome Lattice

The NN kagome lattice consists of three grids of straight parallel filaments intersecting at lattice sites as shown in Fig. 11. This figure also shows two different unit cells reflecting the 3-fold symmetry of the lattice. For the moment, we focus on lattices with $N_x = N_y$ cells on a side as shown in the figure. The equilibrium and dynamical matrices are straightforwardly calculated from it, as are the phonon spectrum and zero modes. As in the square lattice, each of the kagome-lattice filaments supports a SSS under periodic boundary conditions (care must be taken to join equivalent sites at the boundaries to create a single filament for bonds slanting to the left from the bottom), and the expectation is that a periodic lattice will have $3N_x$ states of self stress, and this is indeed the case. There is one state of self stress for each wavevector $\mathbf{q} = q\mathbf{G}_j/G_0$ along the symmetry equivalent lines from Γ to M in the BZ [Fig. 12(a)] parallel to the three reciprocal lattice vectors $\mathbf{G}_j$, where $G_0 = |\mathbf{G}_j| = 4\pi/(\sqrt{3}a)$. Since there are N_x values of $\mathbf{q}$ along each of these directions, there are a total of $3N_x$ SSSs, from which SSS for individual filaments can be constructed.

The $3N_x$ SSSs require an equal number of zero modes, which, as in the square lattice, occur along lines in reciprocal space that have no component parallel to one of the three grids, i.e., along the lines ΓM in reciprocal space as shown in Fig. 12(b). The zero modes for a filament parallel to the x-axis consist of displacements of all 1-sites and 3 sites by $s(\cos\pi/6, \sin\pi/6)$ and $s(\cos\pi/6, -\sin\pi/6)$, respectively, for infinitesimal s. This corre-

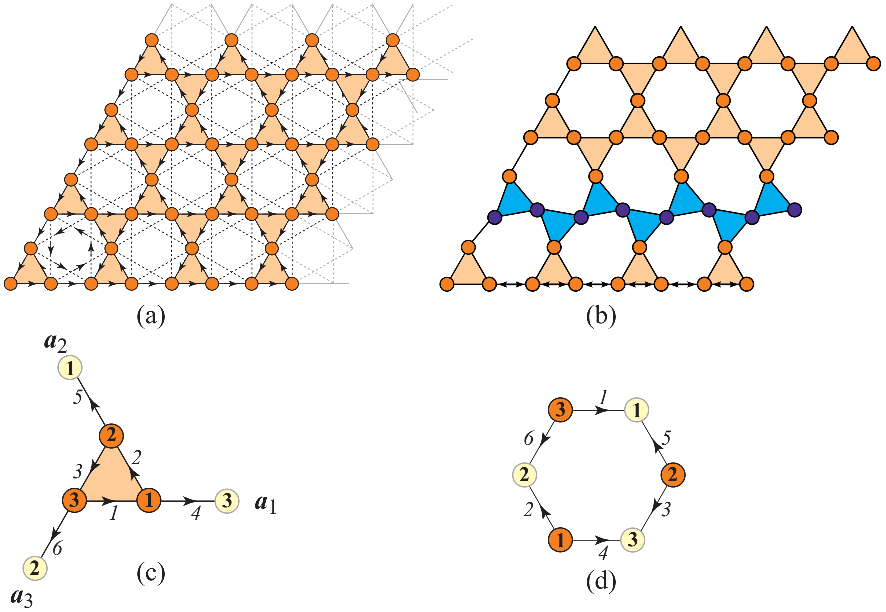

FIG. 11. (a) An $N_x = 5$ by $N_y = 5$ kagome lattice showing NN (full lines) and NNN (dotted lines) bonds. The gray bonds along the right and upper edges are the $2(N_x + N_y - 1)$ NN and $4(N_x + N_y - 1)$ NNN bonds that must be cut from a $N_x \times N_y$ lattice under periodic boundary conditions to produce the the free $N_x \times N_y$ lattice. (b) Representation of a zero modes. (c) and (d) two different symmetric versions of the kagome unit cells showing labeling of sites and NN bonds. The vectors $\boldsymbol{a}_1$ and $\boldsymbol{a}_2$, $\boldsymbol{a}_1$ and $-\boldsymbol{a}_3$, or any other similar pair can serve as basis vectors for the triangular Bravais lattice.

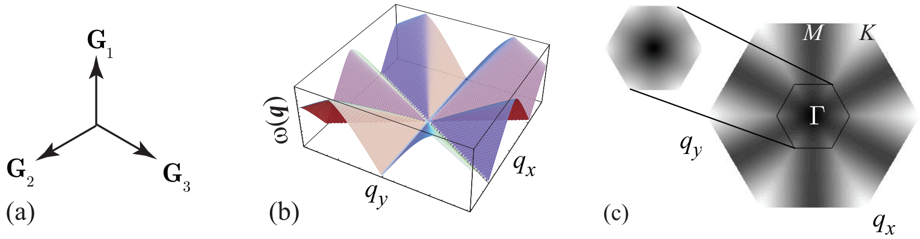

FIG. 12. (a) Shortest reciprocal lattice vectors, related by 3-fold rotations, of the kagome lattice that satisfy $\mathbf{G}_j \cdot \boldsymbol{a}_j = 0$. (b) Dispersion of lowest-frequency mode, showing "knife-edges" along the $\Gamma - M$ in the BZ. (c) Density plot of lowest-frequency mode with $k'/k = 0.02$. Note the isotropic behavior near $\mathbf{q} = 0$.

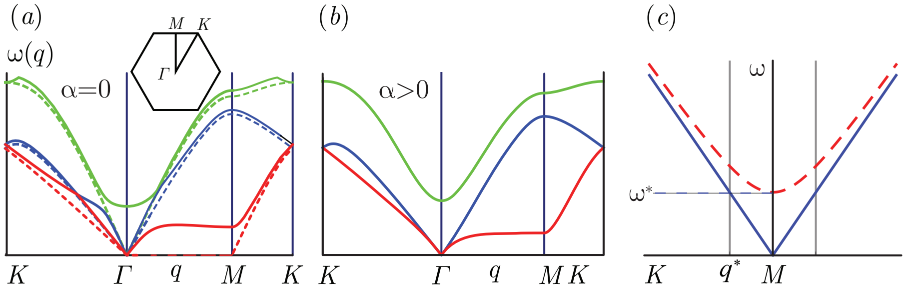

FIG. 13. (a) Phonon spectrum for the three lowest modes of the undistorted kagome lattice. Dashed lines depict frequencies at $k' = 0$ and full lines at $k' > 0$. The inset shows the Brillouin zone with symmetry points Γ, M, and K. (b) Phonon spectrum of the twisted kagome lattice with $\alpha > 0$ and $k' = 0$. (c) Phonon dispersion along the zone edges from K to M in schematic form for both the undistorted lattice at $k' > 0$ and for the twisted lattice with $\alpha \neq 0$, showing the characteristic frequency $\omega^* = 2\sqrt{k'/m}$ ($\omega_\alpha \sim \sqrt{k/m}|\sin\alpha|$) and length $l^* = (q^*)^{-1} = (a/2)(k'/k)^{1/2}$ ($l_\alpha \sim 1/|\sin\alpha|$) for the untwisted (twisted) kagome lattice.

sponds to rigid rotations of triangles about site 2 as shown in Fig. 11(b). An alternative description of the mode is that the entire filament is displaced a distance $s\cos\pi/6$ to the right, and sites 1 and 3 are, respectively, displaced upward and downward a distance $s\sin\pi/6$ producing the zero-modes structure of Fig. 10(b). The spectrum of the lowest-frequency modes has a linear dispersion with $\omega = cq$ ($c = \sqrt{3}ka/8$) in the direction perpendicular to the $\Gamma - M$ zero modes (Fig. 13(c)).

As in the square lattice, adding NNN bonds gaps the spectrum leading to a characteristic frequency $\omega^* \sim \sqrt{k'}$ and associated length scale $\ell^* \sim 1/\sqrt{k'}$ calculated from the dispersion along the line M to K at the zone edge (Fig. 13). Other characteristic frequencies can be calculated from the lowest frequency optical modes or from the frequency at which the low-frequency acoustic phonon modes crosses over to a nearly flat dispersion.

A total of $4N_x - 1$ bonds must be cut to liberate a $N_x \times N_x$-unit-cell free lattice from its periodic parent. There are no states of self-stress in the free lattice, so there must be as many zero modes as bonds that are cut. This is more zero modes than the $3N_x$ in the periodic system. The difference between the two numbers arises from the joining of lines slanting to the left under periodic conditions. The number of horizontal and right slanting filaments is the same in both cases. However, under PBCs, there are N_x distinct left-slanting filaments; under free BCs, there are N_x such lines terminating at the bottom and $N_x - 1$

terminating at the right side of the lattice.

Because of the three sets of filaments aligned along $\boldsymbol{a}_n$, at $\mathbf{q} = 0$, there are now three rather than two SSSs, characterized by bond vectors $\hat{\mathbf{t}}_1 = (1,0,0,1,0,0)/\sqrt{2}$, $\hat{\mathbf{t}}_2 = (0,1,0,0,1,0)/\sqrt{2}$, and $\hat{\mathbf{t}}_1 = (0,0,1,0,0,1)/\sqrt{2}$, each of which has a nonzero overlap with the vector of affine distortions. This gives enough SSSs to fully stabilize the elastic energy of the NN kagome lattice with nonzero Lamé coefficients . Addition of NNN bonds increases these coefficients.

$$\lambda = \mu = \frac{\sqrt{3}}{8}(k + 3k') \tag{5.1}$$

The response is affine even though three sites per unit cell introduces the possibility of their undergoing nonaffine displacement to lower energy. However, the geometry of this lattice is special, and response is necessarily affine .

B. Twisted Kagome Lattice

The twisted kagome lattice is constructed from the finite zero modes by oppositely rotating triangles along all of the filaments of the untwisted lattice through an angle α as shown in Fig. 14. There are a continuum of lattices indexed by the angle α that bond 1 makes with the x-axis. As we shall see, this lattice has properties that at first blush seem surprising but that in fact are simple consequences of the Index theorem .

1. Bulk and elastic properties

The straight filaments of the untwisted kagome lattice become “zigzagged” and lose their ability to sustain SSSs. The result is that there are only the two $\mathbf{q} = 0$ states of self stress required by the Index theorem and the existence of two zero modes of translation, and there are no zero modes other than those at $\mathbf{q} = 0$. Thus the simple rotation of triangles to create a twisted lattice from an untwisted one gaps all but the $\mathbf{q} = 0$ bulk phonons, just as does adding NNN bonds to the untwisted lattice (Fig. 13). The untwisted spectrum is approached continuously as $\alpha \to 0$ leading to a characteristic frequency (measured by the gap at the symmetry point M) and associated length scale,

$$\omega_\alpha \sim |\sin\alpha|, \qquad l_\alpha \sim \frac{1}{|\sin\alpha|}. \tag{5.2}$$

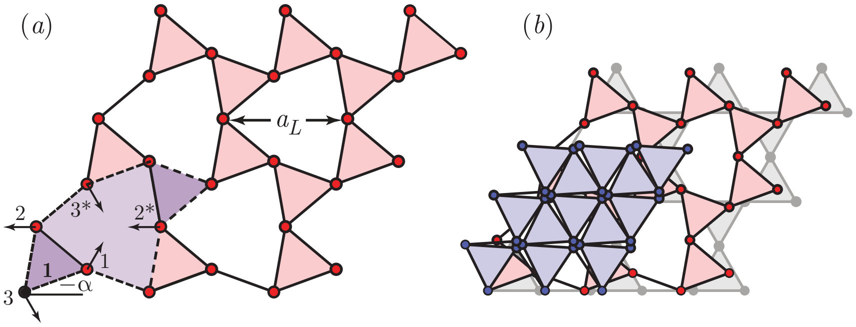

FIG. 14. (a) Twisted kagome lattice showing the displacements of sites in the two unit cells shown in Fig. 11 and rotation of triangles through ±α. Bond **1** (connecting sites 3 and 1) in this figure is rotated through an angle $-\alpha$. The lattice spacing for bonds of length $a/2$ is $a_L = a \cos\alpha$. (b) Lattices with different values of α superposed showing how changing α reduces the lattice area. *From reference*

that, respectively, vanish and diverge as $\alpha \to 0$.

As Fig. 14 shows, twisting the lattice uniformly compresses it. If bond lengths are fixed at $a/2$, the Bravais lattice vectors are reduced in length from a to $a_L = a\cos\alpha$, and the volume of each unit cell from $(\sqrt{3}/2)a^2$ to $(\sqrt{3}/2)a^2\cos^2\alpha$. Thus angle changes modify the area of the lattice without changing any bond length of a NN lattice, implying that the bulk modulus B of these lattices vanishes for all $\alpha \neq 0$. Observe that the twisted lattice has the peculiar property that it expands or contracts isotropically at no energy cost. If it expands in one direction, it will also do so in the opposite direction. Elastic materials with this property have a negative Poisson ratio ; they are *auxetic*. The twisted kagome lattice has the most negative allowed Poisson ratio of −1, which it retains for all strain, and it sometimes called *maximally auxetic* . In addition, the unit cell contracts isotropically. Such lattices are termed *equiauxetic* . There are not many naturally occurring materials that have this property, but artificial ones can be created .

As indicated above, there are two $\mathbf{q} = 0$ states of self-stress that have the potential to create non-vanishing elastic moduli. The long-wavelength elasticity is necessarily isotropic, so if the bulk modulus is zero, the only option is for there to be an isotropic shear modulus or for none of the elastic moduli to be nonzero. The two states of self-stress overlap with affine strain, the shear modulus $\mu = \sqrt{3}k/8$ is nonzero (and curiously independent of α) and identical to that of the untwisted kagome lattice [Eq. (5.1)], and the elastic energy density is

$$f_{\mathrm{el}} = \frac{1}{2}\mu\, \tilde{u}_{ij}\tilde{u}_{ij} \tag{5.3}$$

where $\tilde{u}_{ij} = u_{ij} - \frac{1}{2}u_{kk}$ is the symmetric, traceless shear-strain tensor.

The strain is related to the metric tensor g_{ij} via $u_{ij} = (g_{ij} - \delta_{ij})/2$. The traceless part of the strain, $\tilde{u}_{ij} = (1/2)(g_{ij} - \frac{1}{2}\delta_{ij}g_{kk})$, which is zero for $g_{ij} = \delta_{ij}$, is invariant, and thus remains equal to zero, under conformal transformations that take the metric tensor from its reference form δ_{ij} to $h(\mathbf{x})\delta_{ij}$ for any continuous function $h(\mathbf{x})$ of position $\mathbf{x}$. The zero modes of the theory thus correspond simply to conformal transformations, which in two dimensions are best represented by the complex position and displacement variables $z = x + iy$ and $w(z) = u_x(z) + iu_y(z)$. All conformal transformations are described by an analytic displacement field $w(z)$. Since by Cauchy's theorem, analytic functions in the interior of a domain are determined entirely by their values on the domain's boundary (the "holographic" property), the zero modes of a given sample are simply those analytic functions that satisfy its boundary conditions. For example, a disc with fixed edges ($\mathbf{u} = 0$) has no zero modes because the only analytic function satisfying this FBC is the trivial one $w(z) = 0$; but a disc with free edges (stress and thus strain equal to zero) has one zero mode for each of the analytic functions $w(z) = a_n z^n$ for integers $n \geq 0$. The boundary conditions $\lim_{x\to\infty} \mathbf{u}(x, y) = 0$ and $\mathbf{u}(x, y) = \mathbf{u}(x+L, y)$ on a semi-infinite cylinder with axis along x are satisfied by the function $w(z) = e^{iq_x z} = e^{iq_x x}e^{-q_x y}$ when $q_x = 2n\pi/L$, where n is an integer. This solution is identical to that for classical Rayleigh waves on the same cylinder. Like the Rayleigh theory, the conformal theory puts no restriction on the value of n (or equivalently q_x). Both theories break down, however, at $q_x = q_c \approx \min(l_\alpha^{-1}, a^{-1})$ beyond which the full lattice theory, which yields a complex value of $q_y = q_y' + iq_y''$, is needed.

2. *Surface modes*

As we have seen, free two-dimensional lattices of N sites cut from a periodic Maxwell lattice necessarily have of order $\sqrt{N}$ zero modes because of order $\sqrt{N}$ bonds must be cut, and any sample-spanning states of self stress are lost under the cut. In the untwisted kagome lattice, these modes are identical to the bulk zero modes calculated under PBCs. In the twisted lattice, whose cut lattice must have the same number of zero modes as the untwisted lattice, there are no bulk zero modes (except at $\mathbf{q} = 0$), and as a result the zero modes must be localized at surfaces. In the long-wavelength limit, these modes must reduce to the zero-frequency Rayleigh waves of an isotropic elastic continuum with vanishing bulk modulus with decay length $l_s \equiv \kappa^{-1}$ equal to the inverse surface wavenumber q. At shorter wavelength, l_s is determined by the length l_α associated with the twisted phonon gap.

Figure 15 depicts a finite rectangular sample with free horizontal surfaces parallel to $\boldsymbol{a}_1$ and vertical surfaces parallel to $\boldsymbol{a}_2 - \boldsymbol{a}_3$ along with unit cells constructed so that all sites and bonds on a surface lie in periodically repeated continuous cells. It also shows which bonds (or bonds and sites) must be removed to liberate the finite lattice from the one under PBCs. The removal of two bonds or four bonds and one site per unit cell liberate the horizontal surfaces. In either case, the number of zero modes per cell is $n_0 = 2\Delta n - \Delta n_b = 2$, where $\Delta n = 0$, $\Delta n_b = -2$ in the first case and $\Delta n = -1$, $\Delta n_b = -4$ in the second. Similar arguments yield $n_0 = 4$ for vertical surfaces. As might be expected, the modes are distributed equally between opposite surfaces, i.e., there is one zero mode per unit cell on horizontal surfaces and two modes per unit cell on vertical surfaces. Equivalently, there is one (two) mode per surface wavenumber $-\pi/G_s < q < \pi/G_s$, where G_s is the magnitude of the surface reciprocal lattice vector, $2\pi/a$ for horizontal and $2\pi/(\sqrt{3}a)$ for vertical surfaces.

The amplitude of the surface modes decay as $\exp[-\tilde{\kappa}s]$ with distance s away from the surface all of the way to the opposite free surface, where $\tilde{\kappa}$ is in general complex indicating oscillations along with decay. $\kappa \equiv \operatorname{Re}\tilde{\kappa} = l_s^{-1}$ is the inverse decay length. In the case of horizontal surfaces, the decay length is the same on opposite surfaces. Figure 15(b) plots the single $\kappa(q, \alpha)$ for different values of α. In the case of vertical surfaces, the two decay lengths for the left surface differ from those of the right one. Figure 15(c) plots these for $\alpha = \pi/8$. In all cases, one $\kappa(q, \alpha)$ reduces to $\kappa(q, \alpha) = q$ in the long-wavelength limit as required by the continuum theory.

Surface zero modes are by definition in the null space of the compatibility matrix C. Systems with parallel free surfaces with PBCs along their direction of alignment can be viewed as a series of layers $n = 1, ..., N$, and C can be decomposed as

$$\mathsf{C} = \begin{pmatrix} \mathbf{C}_{11} & \mathbf{C}_{12} & 0 & \dots & 0 & 0 \\ 0 & \mathbf{C}_{11} & \mathbf{C}_{12} & \dots & 0 & 0 \\ \multicolumn{6}{c}{\dotfill} \\ 0 & 0 & 0 & \dots & \mathbf{C}_{11} & \mathbf{C}_{N-1,N} \\ 0 & 0 & 0 & \dots & 0 & \mathbf{C}_{NN} \end{pmatrix}, \tag{5.4}$$

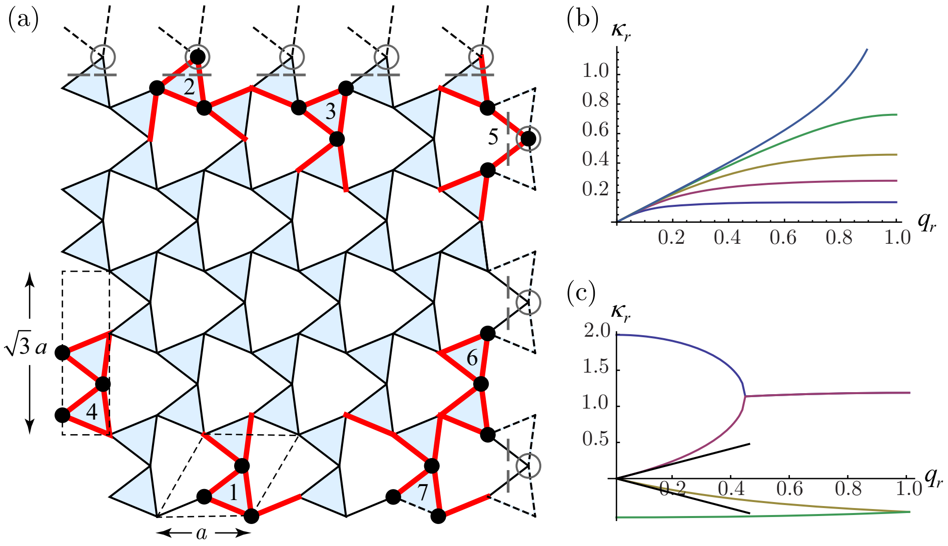

FIG. 15. (color online) (a) A free twisted kagome lattice with free horizontal and vertical boundaries. Sites and bonds of unit cells that match the surface are shown in black and red, respectively, and the geometric form of these unit cells are indicated by dashed quadrilaterals. Cutting the two (four) dashed bonds per cell on the horizontal (vertical) boundary produces a lattice with bottom (left) and top (right) boundary cells 1 (4) and 2 (5). Alternatively removing these bonds along with one circled site and the two bonds crossed by grey lines changes the top (right) boundary cell from 2 (5) to 3 (6). The number of zero modes per site is 1 (2) per site on both the bottom (right) and top (left) boundaries. Cell 7 has one additional bond cut from it. (b) The reduced inverse decay length $\kappa_r = \kappa/(G_r/2)$ of the horizontal boundaries as a function of $q_r = q/(G_r/2)$, where $G_r = 2\pi/a$ for $\alpha = \pi/20, \pi/10, 3\pi/20, \pi/5, \pi/4$ in order from bottom to top. All curves follow $\kappa_r = q_r$ near $q_r = 0$. The curve at $\alpha = \pi/4$ diverges at $q_r = 1.0$. (c) κ_r as a function of q_r with $G_r = 2\pi/\sqrt{3}$ for $\alpha = \pi/8$. The positive curves are for the left boundary and the negative ones are minus κ_r for the right boundary. The two positive curves merge at $q_r \approx 0.4$. There are still two distinct decays beyond this point with the same real part and different imaginary parts. The straight grey lines are the elastic limit $\kappa_r = q_r$.

where all $\mathbf{C}_{ij}$'s depend on the surface wavenumber q and α. $\mathbf{C}_{11}$ is the 6×6 matrix connecting bonds and sites within in a single unit cell and $\mathbf{C}_{12}$ is the 6×6 matrix connecting bonds in one unit cell to sites in unit cells one layer deeper in the sample. The same unit cells are used throughout the sample. The opposite surface may terminate with only a partial version of these cells, and the exact forms of $\mathbf{C}_{N-1,N}$ and $\mathbf{C}_{NN}$ depend on how the surface is terminated. Consider, for example, horizontal surfaces, the bottom of which is characterized by the unit cell labeled 1 in Fig. 15(a) and the top of which is characterized by unit cell 2. For modes localized at the bottom surface, unit cell 1 is used throughout the sample. The termination cell 2 at the opposite surface has all three sites but only four bonds of unit cell 1. The missing bonds (5 and 6) are not affected by cell $N-1$. Therefore, $\mathbf{C}_{N-1,N} = \mathbf{C}_{12}$ is a 6×6 matrix, and $\mathbf{C}_{NN}$ is a 4×6 matrix. If the top surface is terminated by unit cell 3, which has only 2 sites and 2 bonds of cell 1, $\mathbf{C}_{N-1,N}$ is a 6×4 matrix and $\mathbf{C}_{N,N}$ is a 2×4 matrix. Thus displacements $\mathsf{U} = (\mathbf{u}_1, ..., \mathbf{u}_N)$ in the null space of C satisfy

$$\mathbf{C}_{11}\mathbf{u}_n + \mathbf{C}_{12}\mathbf{u}_{n+1} = 0, \tag{5.5}$$

for $n = 1, ...N-2$. These equations are solved by $\mathbf{u}_{n+1} = \lambda \mathbf{u}_n$ and

$$\det(\mathbf{C}_{11} + \lambda \mathbf{C}_{12}) = 0 \tag{5.6}$$

subject to the boundary conditions that $\mathbf{C}_{11}\mathbf{u}_{N-1} + \mathbf{C}_{N-1,N}\mathbf{u}_N = 0$ and $\mathbf{C}_{NN}\mathbf{u}_N = 0$.

The inverse penetration depth is determined by λ via $\exp[-\kappa a_\perp] = \lambda$, where $a_\perp = a\sqrt{3}/2$ is the distance between unit cells in the direction perpendicular to the surface. In case of termination with either unit cell 2 or unit cell 3, $\mathbf{u}_N$ must equal $\lambda \mathbf{u}_{N-1}$ to solve the first boundary condition. Though required by the known existence of the zero mode, it is a remarkable fact that the projection of $\mathbf{u}_1$, which is in the null space of $\mathbf{C}_{11} + \lambda \mathbf{C}_{12}$, onto the space of displacements of the last layer is also in the null space of $\mathbf{C}_{NN}$, and as advertised earlier, the surface mode decays exponentially from one free surface to the next. A similar analysis applies to the vertical surface for which $a_\perp = a/2$. Of course, any linear combination of the exponentially decaying modes on the two sides of a strip is a zero mode if both are individually. In the usual situation in which the Rayleigh waves have a nonzero frequency, the eigenstates of a finite strip are symmetric and anti-symmetric combinations of states on the two surfaces that interact across the strip yielding a peristaltic mode with $\omega \sim q$ and a bending mode with $\omega \sim q^2$. It should be noted that κ for modes that are not localized within the surface unit cell can also be calculated from $\det C(\mathbf{q})$, which is a function of $\exp[i\mathbf{q} \cdot \boldsymbol{a}_i]$, $i = 1, ..., 3$, by setting $\mathbf{q} = q_\perp \hat{\mathbf{n}}_{\text{in}} + \mathbf{q}_{||}$ where $\mathbf{q}_{||}$ is the component of $\mathbf{q}$ parallel to the surface and $\hat{\mathbf{n}}_{\text{in}}$ is the unit inward normal to the surface, setting $q_\perp = i\kappa$, and solving for κ in $\det C(i\kappa, \mathbf{q}_{||}) = 0$. This approach does not directly provide eigenvectors satisfying boundary conditions.

A surface consisting of unit cells 7 in Fig. 15(a) differs from surfaces composed of other unit cells shown in that figure in that it is missing a bond on the surface: it is obtained from cell 1 by cutting the dashed downward pointing bond, and as a result, this surface has two, not one zero mode per cell. The calculation just outlined indeed produces two zero modes per q, one of which is localized completely on the first row because $\mathbf{C}_{11}$ has a non-empty null space. Similarly, κ diverges as shown in Fig. 15(b) at $q = \pi/G_s$ for $\alpha = \pi/4$ because $\mathbf{C}_{11}(\pi/G_s, \pi/4)$ has a non-empty null space.

VI. TOPOLOGICAL EXCITATIONS IN ONE-DIMENSION

Lubensky, T. C., C. L. Kane, Xiaoming Mao, A. Souslov, and Kai Sun. "Phonons and Elasticity in Critically Coordinated Lattices." Reports on progress in physics. Physical Society (Great Britain) 78, no. 7 (2015-Jul 2015): 073901.

A. The Su-Schrieffer-Heeger (SSH) Model

references:

Lubensky, T. C., C. L. Kane, Xiaoming Mao, A. Souslov, and Kai Sun. "Phonons and Elasticity in Critically Coordinated Lattices." Reports on progress in physics. Physical Society (Great Britain) 78, no. 7 (2015-Jul 2015): 073901.

Polyacetylene is a one-dimensional polymer with a $[C_2H_4]$ repeat unit as shown in Figs. 16 (a) and (c). In its ground state, it dimerizes into one of two states with two carbon atoms per unit cell and alternating double and single bonds. When oxidized with halogen vapor, it becomes an excellent conductor, the discovery of which led to the 2000 Nobel Prize in chemistry for Alan J. Heeger, Alan Macdiarmid, and Hideki Shirakawa. This system is the earliest example of a topological phase of matter that we know of. Though deceptively simple, it contains all of the hallmarks of more complex topological phases: it is characterized by a topological winding number or Berry phase , and it has topologically protected edge states both at free boundaries and at walls separating two distinct phases. In addition, there is a one-to-one correspondence between the electronic properties of the spinless Su-

Schrieffer-Heeger (SSH) Model for polyacetylene vibrational properties of a one-dimensional model topological mechanical system, which we will review shortly.

In the dimerized state, the SSH Hamiltonian can be expressed as

$$H = \sum_s [v_1(\psi^\dagger_{A,s}\psi_{B,s} + \psi^\dagger_{B,s}\psi_{A,s}) - v_2(\psi^\dagger_{A,s}\psi_{B,s-1} + \psi^\dagger_{B,s-1}\psi_{A,s})] \tag{6.1}$$

$$= \sum_s \Psi^\dagger_s H_{s,s'} \Psi'_s = \sum_{s,s'} [\psi^\dagger_{A,s} Q_{s,s'} \psi_{B,s'} + \psi^\dagger_{B,s} C_{s,s'} \psi_{A,s'}] = \frac{1}{N}\sum_q \Psi^\dagger(\mathbf{q}) H(\mathbf{q}) \Psi(\mathbf{q}) \tag{6.2}$$

where s specifies the position of each two-cite unit cell, N is the number of cells, v_1 is the hopping matrix element from an A site on the left to a B-site on the right and v_2 the matrix element from a B-site on the left to an A-site on the right, $\Psi_s = (\psi_{A,s}, \psi_{B,s})$ and

$$H = \begin{pmatrix} 0 & v_1 \delta s s' - v_2 \delta_{s-1,s'} \\ v_1 \delta_{ss'} - v_2 \delta_{s+1,s'} & 0 \end{pmatrix} \equiv \begin{pmatrix} 0 & Q_{s,s'} \\ C_{s,s'} & 0 \end{pmatrix}. \tag{6.3}$$

We will refer to the phase with $|v_2| > |v_1|$ as the "plus" phase and that with $|v_2| < |v_1|$ as the "minus" phase [Fig. 16(c)]. Thus, the plus phase can be converted to a minus phase interchanging v_1 and v_2.The Fourier transformed version of H is

$$H(q) = \begin{pmatrix} 0 & C^*(q) \\ C(q) & 0 \end{pmatrix}, \tag{6.4}$$

where

$$C(q) = v_1 - v_2 e^{iqa}. \tag{6.5}$$

The eigen-energies as a function of wavenumber q are simply

$$E(q) = \pm|C(q)| = \pm\sqrt{(v_1 - v_2)^2 + 4 v_1 v_2 \cos^2(qa/2)}, \tag{6.6}$$

where a is the lattice spacing of the dimerized lattice, i.e., the distance between neighboring A (or B) sites. In the undimerzied system, $v_1 = v_2$ and $E(q) = \pm|v_1||\cos qa/2|$, where a is the unit cell length, yielding two bands that meet linearly at $q = \pm\pi/a$, i.e., at the band edges. When $v_1 \neq v_2$, a gap of magnitude $\Delta E = 2|v_1 - v_2|$ develops at $q = \pm\pi$.

The dynamical equations for ψ_A and ψ_B are

$$C_{ss'}\psi_{A,s'} = v_1\psi_{A,s} - v_2\psi_{A,s+1} = E\psi_{B,s} \tag{6.7}$$

$$Q_{ss'}\psi_{B,s'} = v_1\psi_{B,s} - v_2\psi_{B,s-1} = E\psi_{A,s}. \tag{6.8}$$

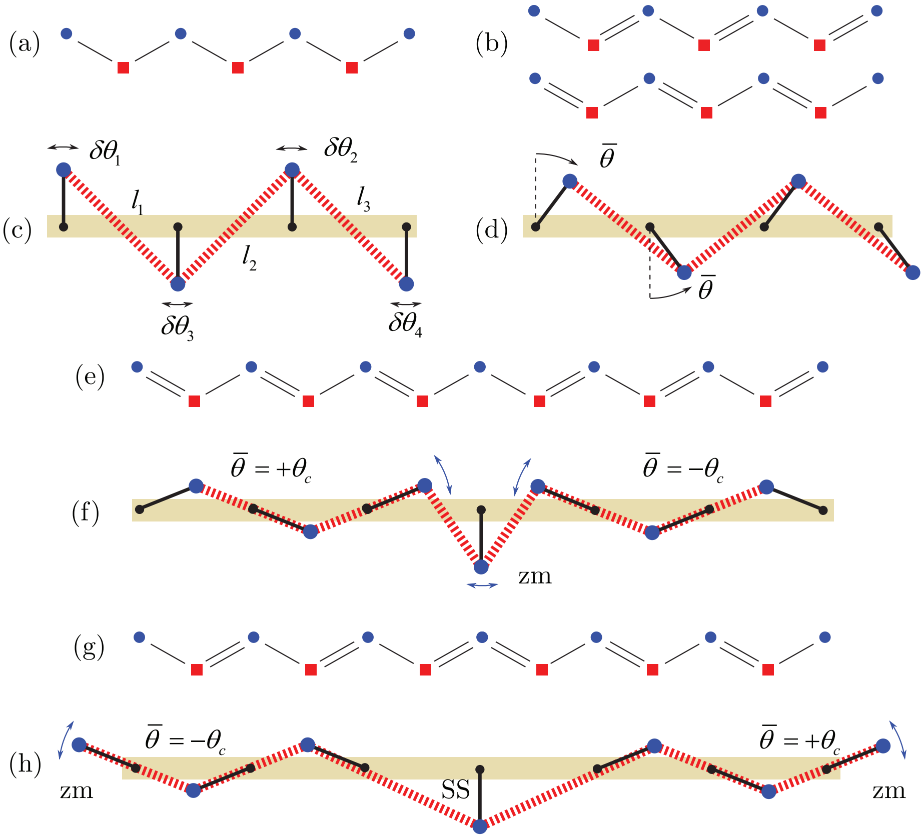

FIG. 16. (a) An undimerized polyacetylene lattice showing A sites as blue circles and B sites as red squares. (b) Top: the "plus" dimerized phase in which the weaker single-orbital bond connects an A site to the left to a B site to the right and the stronger two-orbital bonds connects a B sit to the left with an A site to the right; Bottom the "minus" phase in which the strong and weak bonds are interchanged. (c) The associated untilted mechanical lattice in which masses, represented by the larger blue dots, are connected by springs in red and are constrained by rigid rods to rotate about fixed pivot points, represented by small black dots. The masses can be identified with the *A*-sites in polyacetylene and the springs with the *B*-sites. (d) Mechanical lattice associated with the "minus" polyacetylene lattice. (e) A domain wall in polyacetylene connecting a "minus lattice on the left with a "plus" lattice on the right with a zero-mode in the A lattice. (f) Representation of the same domain wall in the mechanical lattice. (g) Polyacetylene domain wall connecting a "plus" lattice on the left to a "minus" lattice on the right. This lattice has B-lattice zero mode associated with the domain wall and two A-lattice zero modes at the two edges. (h) Mechanical lattice analog of (g) with a state of self stress on the domain wall and two zero modes at the two edges.

Note that when $E = 0$ the equations for $\psi_{B,s}$ and $\psi_{A,s}$ decouple completely, so there will be zero-energy states with non-zero amplitude only on the A-lattice and ones with non-zero amplitudes only on the B-lattice. The wave functions for the zero modes are obtained by setting the energy E equal to zero. Then

$$\psi_{A,s+1} = \frac{v_1}{v_2}\psi_{A,s} \Rightarrow \psi_{A,s} = \left(\frac{v_1}{v_2}\right)^s \psi_{A,0}. \tag{6.9}$$

Thus, there is a zero-energy state originating at the left end and decaying to the right. If $|v_1| > |v_2|$, this state cannot exist because it would grow exponentially to the right. In this case, a zero-energy state exists on the right edge, which can be seen by rewriting Eq. (6.9) as

$$\psi_{A,s-1} = \frac{v_2}{v_1}\psi_{A,s} \Rightarrow \psi_{A,N-s} = \left(\frac{v_2}{v_1}\right)^s \psi_{A,N} \tag{6.10}$$

This corresponds to a zero mode decaying from the right boundary when $|v_2| < |v_1|$ The B-lattice equations imply

$$\psi_{B,N-s} = \left(\frac{v_1}{v_2}\right)^s \psi_{B,N} \tag{6.11}$$

$$\psi_{B,s} = \left(\frac{v_2}{v_1}\right)^s \psi_{B,0} \tag{6.12}$$

corresponding to zero-energy right edge state when $|v_1| < |v_2|$ and left edge state when $|v_1| > |v_2|$.

The existence of edge states is intimately connected with the topological properties of the energy spectrum, in particular with zeros and poles of $C(q)$ as a function of $z = e^{iqa}$. To see how this comes about, we introduce the topological winding number associated with any function $\Phi(\mathbf{q})$ of vectors $\mathbf{q}$ in a Brillouin zone:

$$n_\Phi(\mathbf{G}) = \frac{1}{2\pi i}\int_0^{\mathbf{G}} d\mathbf{q}\cdot\nabla_{\mathbf{q}} \ln \Phi(\mathbf{q}) \equiv \frac{1}{2\pi i}\int_0^{G} dq \frac{d\ln\Phi(q)}{dq}, \tag{6.13}$$

associated with the reciprocal lattice vector $\mathbf{G} = p\boldsymbol{b} = G\mathbf{e}_x$, where $\mathbf{e}_x$ is the unit vector along x, $\boldsymbol{b} = (2\pi/a)\mathbf{e}_x$, $p = \pm1, \pm2, \cdots$, and $\mathbf{q} = q\mathbf{e}_x$. Though it is not necessary to introduce vectors in this one-dimensional example, it is useful to do so in preparation for our treatment of higher-dimensional systems in the next section. This leads naturally to a topological number associated with $C(\mathbf{q})$: $n_C(\mathbf{G}) = pn_C(\boldsymbol{b})$ for any $\mathbf{G} = p\boldsymbol{b}$, where $\boldsymbol{b} = (2\pi/a)\mathbf{e}_x$, $p = \pm1, \pm2, \cdot$, and

$$n_C(\boldsymbol{b}) \equiv n_C = \frac{1}{2\pi i}\int_0^{2\pi/a} dq \frac{d}{dq}\ln C(q) = \frac{1}{2\pi i}\oint_\Gamma dz \frac{d}{dz}\ln C(z) = n_{C,0} - n_{C,p}, \tag{6.14}$$

where Γ is the contour $|z| = 1$, $z = e^{iqa}$, and $n_{C,0}$ and $n_{C,p}$ are, respectively, the number of zeros and the number of poles in $C(z)$ within the unit circle $|z| = 1$. When $|v_1| < |v_2|$, $C(z)$ has one zero and no poles interior to Γ, and $n_C = +1$. When $|v_2| < |v_1|$, $C(z)$ has no zeros or poles interior to Γ, and $n_C = 0$.

In preparation for our treatment of higher-dimensional topological systems, it is useful to introduce at this point a topological polarization vector $\mathbf{R}_T$ as follows: First define

$$h = -n_C(\boldsymbol{b}) \tag{6.15}$$

and

$$\mathbf{R}_T = h\boldsymbol{a}, \tag{6.16}$$

where

$$\boldsymbol{a} = a\mathbf{e}_x \tag{6.17}$$

is the lattice vector. Then $h = -1$ when $|v_1| < |v_2|$, and $h = 0$ for $|v_1| > |v_2|$. Thus

$$C(\mathbf{q}) = |C(\mathbf{q})|e^{-i\mathbf{q}\cdot\mathbf{R}_T} \tag{6.18}$$

where $\mathbf{q} = q\mathbf{e}_x$. n_C is the number of ZMs on the left edge. [Note the minus sign in Eq. (6.15). This definition is chosen to correspond closely to what is found in the quantum topological literature, where the distinction between C and Q is less important.] The general topological number $n_C(\mathbf{G})$, where $\mathbf{G}$ is the *outward* pointing reciprocal lattice defining the surface lattice plane, is then

$$n_C(\mathbf{G}) = \mathbf{G} \cdot \mathbf{R}_T/(2\pi), \tag{6.19}$$

In the current example, $n_C(\boldsymbol{b}) = 1$ and $\mathbf{G} = -\boldsymbol{b}$ for the left edge, and $+\boldsymbol{b}$ for the right edge, yielding $n_C(\mathbf{G}) = +1$ for the left edge and $n_C(\mathbf{G}) = -1$ for the right edge for the "plus" phase and zero at both ends for the "minus" phase.

It would seem that the number of ZMs on the right edge should be $n_C(\boldsymbol{b}) = -n_C(-\boldsymbol{b})$, but this is clearly incorrect because $n_C(-\boldsymbol{b}) = 0$ when $|v_1| > |v_2|$. The problem is that we need a "backward" rather than a "forward" C to describe modes localized on the right. To create a "backward" C, we have only to reassign sites and/or bonds to convert the "left-compatible" A-terminus unit cell, with A to the left of B to a "right-compatible" one, with A to the right of B (and similarly for B-terminus unit cells). Define $\psi'_{A,s} = \bar{\psi}^{\dagger}_{A,s+\sigma}$ and $\psi'_{B,s} = \psi'_{B,s+\tau}$ where $\sigma = \pm 1$ and $\tau = \pm 1$ such that $\sigma = +1$ converts the left compatible

A-terminus cell to a right compatible one and $\tau = +1$ does the same thing for B-terminus cells. Then Eq. (6.7) becomes $E\psi'_{B,s-\tau} = v_1\psi'_{A,s-\sigma} - v_2\psi'_{A,s+1-\sigma}$, and

$$C'(q) = e^{-i(\sigma-\tau)qa}C(q) \equiv e^{-i\mathbf{q}\cdot\mathbf{R}_L}C(\mathbf{q}) = |C(\mathbf{q})|e^{-i\mathbf{q}\cdot(\mathbf{R}_L+\mathbf{R}_T)}, \tag{6.20}$$

where $\mathbf{q} = q\mathbf{e}_x$, $\mathbf{R}_L = \Delta\vec{r}_A - \Delta\vec{r}_B$, where $\Delta\vec{r}_A = \sigma\boldsymbol{a}$ and $\Delta\vec{r}_B = \tau\boldsymbol{a}$ are the amounts by which A and B are displaced to create a new unit cell as depicted in Fig. 17. For $C'(q)$ to be "backward", it must contain no positive powers of e^{iqa}, which is accomplished by choosing $\sigma - \tau = 1$ (or equivalently $\mathbf{R}_L = \boldsymbol{a}$) so that $C'(q) = v_1 e^{-iqa} - v_2$. $C'(q)$ has no pole and a single zero within the unit circle of the complex $z' = e^{-iqa}$ plane, $|z'| = 1$, when $|v_2| < |v_1|$ and no pole or zero when $|v_2| > |v_1|$. The result is $n_{C'}(-\boldsymbol{b}) = 1$ if $|v_1| > |v_2|$ and $n_{C'}(-\boldsymbol{b}) = 0$ if $|v_1| < |v_2|$, and $n_{C'}(-\boldsymbol{b})$ correctly reproduces the zero-mode count of the right edge. These results can be summarized in a simple formula for the number of ZMs at an edge with *outward* normal $\mathbf{G}$:

$$n_0(\mathbf{G}) = \mathbf{G}\cdot(\mathbf{R}_L^{\mathbf{G}} + \mathbf{R}_T)/2\pi, \tag{6.21}$$

where $\mathbf{G} = -\boldsymbol{b}$ ($\mathbf{G} = \boldsymbol{b}$) on the left (right) edge and $\mathbf{R}_L^G$ is a kind of "surface polarization" that has the same value (0 on the left and $\boldsymbol{a}$ on the right) in the plus and minus phases. Thus in the plus phase when $|v_1| < |v_2|$, $\mathbf{R}_T = -\boldsymbol{a}$, and $n_0(\mathbf{G}) = -\boldsymbol{b}\cdot(-\boldsymbol{a})/(2\pi) = 1$ on the left edge and $n_0(\mathbf{G}) = \boldsymbol{b}\cdot(\boldsymbol{a}-\boldsymbol{a})/(2\pi) = 0$ on the right edge. Both $\mathbf{R}_T$ and $\mathbf{R}_L^{\mathbf{G}}$ depend on the original unit cell choice, but $n_0(\mathbf{G})$ does not. Thus, for the plus phase, n_0 equals one the left and zero on the right edge in agreement with the direct calculation. In the "minus" phase, $\mathbf{R}_T = 0$, but $\mathbf{R}_L$ remains 0 on the left and $\boldsymbol{a}$ on the right, yielding an n_0("minus") of zero on the left and one of the right.

Zero energy states can also exist at domain walls such as that shown in Figs. 16 (e) and (g). In (e), the center of the domain wall is an A-site bounded on the right by a "plus" phase starting with a week bond and on the left by a "minus" phase starting also with a weak bond. Splitting this configuration in two and terminating the freed weak bonds with A-sites creates independent "plus" and "minus" chains, the former with a zero-energy left edge mode and the latter with a zero-energy right edge mode, each with an independent amplitude. When the two terminating A-sites are joined the amplitudes of the two edge modes are locked together, but their zero energy configuration is retained - this is then a zero-energy mode at a domain wall. Obviously, there is only one mode in this case. One way

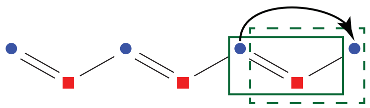

FIG. 17. represetation of a unit cell change brought about by shifting the A-site one unit cell over in a "minus" lattice. The initial cell starts with a A site on the left connected to a B site on its right with a weak bond on the left and a strong one on the right. This cell is appropriate for the description of an edge state on the left edge. The new cell terminates with an A site connected on the left to a B site and the left with the strong bond on the left and weak bond on the right appropriate for the description of an edge state on the right.

to reach this conclusion is to start with the separated lattice, each of which has a zero-energy edge mode. This provides two degress of freedom, $N_L = N_R = 1$. Tying the two A-sites together constitutes a single constraint constraint, $N_C = 1$. There is no analog of states of self stress here, so the Maxwell-Calladine reads $N_0 = N_R + N_L - N_C = 1$ in agreement with our direct construction. This result can be re-expressed in terms of the topological polarizations: $N_R = \mathbf{G} \cdot (\mathbf{R}_L^{+L} + \mathbf{R}_T^R)/(2\pi)$ and $N_L = -\mathbf{G} \cdot (\mathbf{R}_L^{-R} + \mathbf{R}_T^L)/(2\pi)$, where $\mathbf{G} = -\boldsymbol{b}$ is the outer normal to the right chain, and $\mathbf{R}_L^{\pm L(R}$ is the local polarization of the left (or right) edge of the "plus" or "minus" phase and $\mathbf{R}_T^{L(R)}$ is the topological polarization of the left or right phase of the grain boundary. For the case shown in Fig. 16(e) with a "plus" phase on the right and "minus" phase on the left, we have $\mathbf{R}_T^R = \mathbf{R}_T^+ = -\boldsymbol{a}$, $\mathbf{R}_T^L = \mathbf{R}_T^- = 0$, $\mathbf{R}_L^{+L} = 0$ and $\mathbf{R}_L^{-R} = \boldsymbol{a}$. Thus, the Maxwell-Calladine equation becomes,

$$\begin{aligned} N_0 = N_R + N_L - N_C &= \mathbf{G} \cdot (\mathbf{R}_T^L - \mathbf{R}_T^L)/(2\pi) + \mathbf{G} \cdot (\mathbf{R}_L^{+L} - \mathbf{R}_L^{-R})/(2\pi) - N_C \\ &= \mathbf{G} \cdot (\mathbf{R}_T^R - \mathbf{R}_T^L)/(2\pi). \end{aligned} \tag{6.22}$$

This result is general. More general proofs exist, but they are somewhat tedious, and we will not cover them here. The domain wall in Fig. 16(e) harbors a zero mode on the B-lattice. If we remove the double orbitals connecting B-sites to the central A-site at position $s = 0$, then we have a zero-energy mode to the right for $s \geq 1$ starting at the left B-site boundary of the right chain and one decaying to the left for $s < -1$ starting at the right B-site boundary of the left chain. Adding back the broken bonds set $\psi_{B,-1} = \psi_{B+1}$, whih again constitutes a constraint and giving us one zero mode tied to the domain wall.

B. A One-dimensional Mechanical SSH Model

Reference:

Kane, C. L., and T. C. Lubensky. "Topological Boundary Modes in Isostatic Lattices." Nature Physics 10, no. 1 (Jan 2014): 39-45.

Figure 16 depicts a model whose energy dispersion and edge states reproduce those of the SHH model. It consists of rigid bars of length r that can rotate freely about fixed positions, separated by a distance a, on a one-dimensional periodic lattice. The ends of neighboring bars are connected by harmonic springs whose lengths are adjusted so that the equilibrium configuration is one in which alternate rods make an angle $\bar{\theta}$ with the upward or downward normals. We will refer to lattices with bars that tilt to the left with $\bar{\theta} > 0$ and ones with bars that tilt to the right with $\bar{\theta} < 0$ as plus and minus phases, respectively. As we shall see, these two phases have a fully gapped spectrum that is identical to those of the dimerized SSH model: one cannot be converted to the other without closing the gap, and they are topologically distinct. Each rod s has one degree of freedom $\theta_s = \bar{\theta} + \phi_s$, and each spring provides one constraint; under PBCs the number of degrees of freedom match the number of constraints, and this is a Maxwell lattice.

The energy of this system is

$$U = \frac{1}{2} k \sum_s [-L(\theta_s, \theta_{s+1}) + L_0(\bar{\theta})]^2 \equiv \frac{1}{2} k \sum_s e_s^2, \tag{6.23}$$

where e_s is the extension of bond s connecting site s to $s+1$, and

$$L^2(\theta, \theta') = a^2 + 2\,r(\sin\theta' - \sin\theta) + 2r^2[1 + \cos(\theta + \theta')]. \tag{6.24}$$

In the equilibrium state, $\theta_s = \bar{\theta}$ for all s, and the equilibrium spring length is

$$L_0^2(\bar{\theta}) = L^2(\bar{\theta}, \bar{\theta}) = a^2 + 4r^2 \cos^2 \bar{\theta}. \tag{6.25}$$

In the linearized limit,

$$e_s = v_1 \phi_s - v_2 \phi_{s+1} = C_{s,s'} \phi'_s \tag{6.26}$$

the tension on each spring is $t_s = \partial U / \partial e_s = k e_s$, and the "force" at each site is

$$f_s = \partial U / \partial \phi_s = k(v_1 e_s - v_2 e_{s-1}) = v_1 t_s - v_2 t_{s-1} = Q_{s,s'} t'_s \tag{6.27}$$

where

$$v_{1,2} = \frac{(a \pm 2r\sin\bar{\theta})r\cos\bar{\theta}}{\sqrt{a^2 + 4r^2\cos^2\bar{\theta}}}. \tag{6.28}$$

Thus ϕ_s plays the role of $\psi_{A,s}$and e_s plays the role of $\psi_{B,s}$ in the SSH model. The functions C and Q expressed in terms of v_1 and v_2 are identical to the same functions of the SSH model. The energy is also identical to that [Eq. (6.6)] of the SSH model with a gap in the spectrum at $qa = \pi$ when $v_1 \neq v_2$. This implies that the the edge states in ϕ_s are identical to those in $\phi_{A,s}$. The stretches e_s, which reside in the springs that cannot terminate the chain do not exhibit true edge states.

The removal of one spring from a lattice under PBCs creates a finite lattice with two free ends and a deficiency of one spring relative to the Maxwell limit. The finite lattice must terminate at both ends with a mass and not a spring; i.e, it terminates on the left with a "left compatible" unit cell with mass to the left and spring to the right and on the right with a "right compatible" unit cell with spring to the left and mass to the right. The Index Theory then requires that there be one ZM. Since the bulk spectrum is fully gapped and not affected by the spring removal, the ZM must reside at one free edge or the other of the finite lattice. Angles ϕ_s in any ZM must be in the null space of C, and thus satisfy $\phi_{s+1} = (v_1/v_2)\phi_s$, which describes a ZM localized at the left (right) edge and decaying to the right (left) when $|v_2| > |v_1|$ ($|v_2| < |v_1|$). Changing the sign of $\bar{\theta}$ effectively interchanges v_1 and v_2, so that plus and minus phases have a ZM on opposite edges. As long as $2r\sin\bar{\theta} < a$, both v_1 and v_2 are positive and ϕ_n decays monotonically with distance. When $2r\sin\bar{\theta} > a$, ϕ_n will oscillate as well as decay with distance. At the critical angle $\bar{\theta}_c = \sin^{-1}(a/2r)$, $v_1 = 0$, and the left edge state is localized entirely on one edge site. Figure **??**(b) shows these critical states at the two edges. There are no SSSs at free edges because a spring must connect two sites. Localized SSSs as well as ZMs can also exist at domain walls separating chains with opposites signs of $\bar{\theta}$. Figure **??**(a) shows a domain-wall ZM, and Fig. **??** (c) shows an SSS along with two edge ZMs for $\bar{\theta} = \pm\bar{\theta}_c$. The Index Theorem requires $N_0 = N_s$, i.e., one interior SSS domain wall for each ZM domain wall, under PBCs and $N_0 = N_s + 1$ for free boundary conditions. When $\bar{\theta} \neq \pm\bar{\theta}_c$, domain-wall SSSs interact with an exponentially decaying force with domain-wall or edge ZMs and raise their energy from zero.

As we discussed, domain walls separating the plus and minus phases also harbor topologically protected ZMs as shown in Fig. **??**. The number of ZMs minus the number of SSSs per unit cell at domains wall is conveniently expressed as

$$n_0^D - n_s^D = \mathbf{G}^R \cdot (\mathbf{R}_T^R - \mathbf{R}_T^L)/(2\pi), \tag{6.29}$$

where $\mathbf{G}^R$ is the outer normal vector to the edge of right phase and $\mathbf{R}_T^R$ and $\mathbf{R}_T^L$ are the topological polarizations of the right and left phases, respectively.

Our discussion until now focused on the linearized limit of the SSH mechanical chains, which have ZMs localized on the right or left edge. What happens at nonlinear order? The answer is that an initially localized edge mode can move about the chain with arbitrarily small energy cost: the edge mode is converted into a nonlinear topological kink, even in the limit of infinitely rigid springs ($k \to \infty$). There are three versions of this soliton; (1) the flipper, which occurs for $2r\sin\bar{\theta} < 1$ for which $u(x,t) = r\sin\theta(x,t)$ takes the form of a Lorentz-boosted tanh kink and for which θ never exceeds $\bar{\theta}$; (2) The spinner, which occurs for $r\sin^2\bar{\theta} > a$ for which $\cos(\theta - \bar{\theta})$ takes the form of a Lorentz-boosted tanh kink, and (3) the wobbling flipper, which exists for $1 < 2r\sin\bar{\theta} < 2/\sin\bar{\theta}$ and adds periodic oscillations to the flipper solution. What sets these kinks apart from traditional ϕ^4 and sine-Gordon ones is that the kink has zero energy but the anti-kink does not. This feature follows from boundary terms proportional to $d\theta/dx$ that break reflection symmetry. When $2r\sin\bar{\theta} > 1$, neighboring bars can cross each other if they are restricted to the same plane. They can cross, however, if the rotors are placed in different planes as shown in Ref. .

VII. MECHANICAL GRAPHENE

Reference:

Socolar, TCL, Kane, *New J. Phys.* 19 (2017) 025003.

Here, we introduce and explore the properties of a model mechanical system whose bulk vibrational excitations are in correspondence with the electronic excitations of the particle-hole symmetric two-band tight-binding model of graphene. We consider a generalized graphene model describing nearest neighbor hopping on a honeycomb lattice in which the hopping matrix elements for the three bonds emanating from a given site are in general different. This model can represent strained graphene for modest variations in the hopping amplitudes, and also arises in the analysis of Kitaev's honeycomb lattice model . Our mechanical analog is constructed by closely following the paradigm used in the construction of the SSH analog. The honeycomb lattice of graphene, like the 1D SSH lattice, is bipartite with A- and B-sublattices, shown as red and blue disks in Fig. 18. Since there is only one degree of freedom per site in the graphene model, we assign a scalar variable $z(\mathbf{R}_A)$, which we identify as vertical height displacement, to each site on the A-sublattice, and we assign a kinetic energy $\dot{z}^2(\mathbf{R}_A)/2$ to that site. On each site in the B-sublattice, we need to assign the analog of a bond connecting sites on the A-sublattice, but this "bond" is connected to three rather than the usual two sites. To each of these triangular bonds, which we call *tri-bonds*, we assign a kind of "stretching" energy that depends quadratically on a certain linear combination of the heights at the three sites. Figure 18 shows our model mechanical graphene lattice, with red sites representing the locations of the height variables and gray triangles representing the tri-bonds.

The tri-bonds are the analogs of springs in a standard ball-and-spring lattice, and each imposes a constraint that leads to a generalization of the Maxwell-Calladine theorem relating the numbers of zero modes and states of self stress (SSS) to the number of degrees of freedom and number of constraints. Under periodic boundary conditions, our mechanical graphene lattice is a generalized Maxwell lattice in which the number of constraints equals the number of degrees of freedom, and it exhibits all of the properties of ball-and-spring Maxwell lattices: (1) Each zero mode in the bulk spectrum, which again matches the electronic spectrum of graphene, is accompanied by a SSS. (2) Each lattice is characterized by a topological polarization or by Weyl modes. (3) Periodic strips or finite lattices cut from a periodic lattice whose spectrum is fully gapped have a number of zero-frequency surface modes equal to the number of tri-bonds cut, i.e., at least one zero mode per surface wavenumber, residing on one or the other of the opposite free edges. (4) The number of zero modes at a given wavenumber on a free surface is determined by the topological polarization or by the positions of Weyl modes and by a local surface polarization. (5) Domain walls connecting lattices of different topological polarization harbor either zero modes or self stress for each wavenumber along the wall; those connecting different Weyl lattices have zero modes or states of self stress for some wavenumbers but not for others.

Though the bulk spectrum of our model and graphene are identical, their surfaces modes are not. The top and bottom edges of a horizontal strip of the mechanical lattice, which can be created by removing the row of horizontal of dashed tri-bonds in Figure 18 from a periodic lattice, are different: the top surface exposes tri-bond vertices and the bottom a

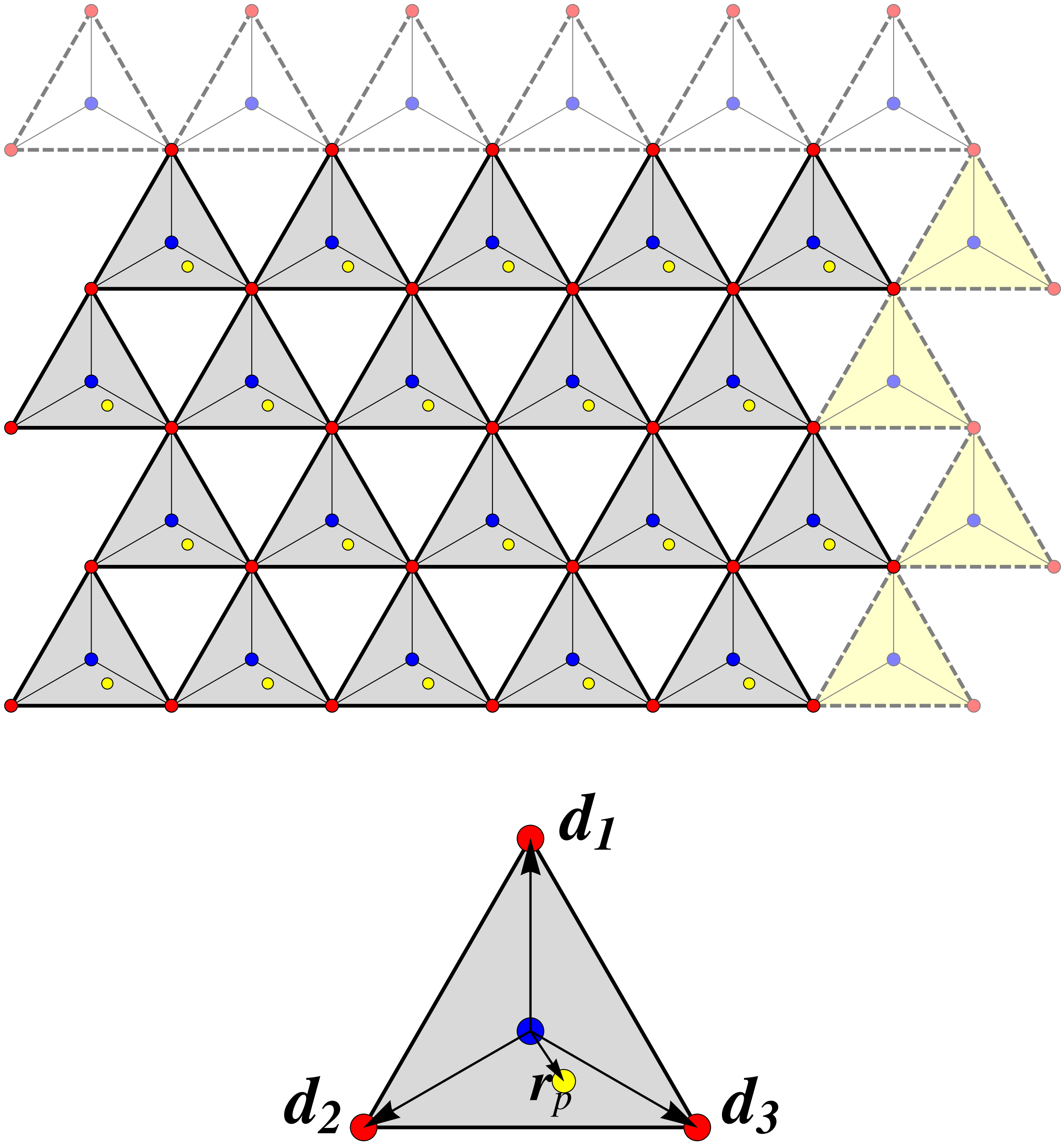

FIG. 18. Top: The tri-bond lattice. Each shaded triangle represents a tri-bond centered on a B site of the graphene lattice (blue disks). The tri-bonds are connected at their vertices, which lie on A-sublattice (red disks). The yellow disk in each tri-bond marks the pivot point. Dashed tri-bonds are those that are cut to create free surfaces. Bottom: A single tri-bond. The pivot point $\vec{r}_p$ is at $(x_1\boldsymbol{d}_1 + x_2\boldsymbol{d}_2 + x_3\boldsymbol{d}_3)$.

straight continuous line of tri-bond edges. These two surfaces correspond, respectively, to the bearded (with dangling bonds) and zigzag edges of graphene . It is not possible to create a strip in the mechanical lattice like that in graphene in which both edges are zigzagged. Both edges of vertical strips exhibit a two-tri-bond zigzag pattern. The corresponding graphene edges correspond to armchair edges with an extra dangling bond at every second row.

A. Model Details

Figure 18 provides a visual image of our model. We take the Bravais lattice constant to be a and define primitive reciprocal lattice vectors

$$\mathbf{a}_1 = a\hat{x}, \tag{7.1}$$

$$\mathbf{a}_2 = a\left(-\frac{1}{2}\hat{x} + \frac{\sqrt{3}}{2}\hat{y}\right), \tag{7.2}$$

$$\mathbf{a}_3 = a\left(-\frac{1}{2}\hat{x} - \frac{\sqrt{3}}{2}\hat{y}\right). \tag{7.3}$$

We also define the three vectors from a tri-bond centroid to its vertices:

$$\mathbf{d}_1 = \frac{a}{\sqrt{3}}\hat{y} \tag{7.4}$$

$$\mathbf{d}_2 = \frac{a}{\sqrt{3}}\left(-\frac{\sqrt{3}}{2}\hat{x} - \frac{1}{2}\hat{y}\right) \tag{7.5}$$

$$\mathbf{d}_3 = \frac{a}{\sqrt{3}}\left(\frac{\sqrt{3}}{2}\hat{x} - \frac{1}{2}\hat{y}\right). \tag{7.6}$$

The centroids of the tri-bonds are located on B sites of the honeycomb and their vertices lie at A sites. Each site on the A-sublattice is occupied by a unit mass that is constrained (say by a frictionless rod) to move in the vertical direction. We assume these vertical displacements $z(\mathbf{R}_A)$ are small enough that linear approximations can be used. Each tri-bond is pinned at a pivot point that is displaced from its centroid by

$$\vec{r}_p = x_1\boldsymbol{d}_1 + x_2\boldsymbol{d}_2 + x_3\boldsymbol{d}_3, \tag{7.7}$$

and the three tri-bonds meeting at a given site are connected in a way that allows each to freely rotate about an axis passing through its pivot point and the site in question.

Any location of the pivot point (within or outside the triangle spanned by the tri-bond vertices) can be specified by a unique triple $x = (x_1, x_2, x_3)$ with $x_1 + x_2 + x_3 = 1$. With this parametrization, the condition

$$e(\mathbf{R}_B) \equiv \sum_{i=1}^{3} x_i z(\mathbf{R}_B + \boldsymbol{d}_i) = 0, \tag{7.8}$$

is satisfied for any rigid rotation of the tri-bond, where $\mathbf{R}_B$ is the B-sublattice location of the tri-bond centroid and $\mathbf{R}_B + \boldsymbol{d}_i$ are the A-sublattice positions of the vertices of the tri-bond. Violation of this condition requires a distortion of the tri-bond that costs some energy. Letting $\mathbf{u}_i = (\boldsymbol{d}_i + z_i \hat{\boldsymbol{z}}) - \vec{r}_p$ denote the vector from the pivot point to vertex i, it is straightforward to check that for a given tri-bond at $\mathbf{R}_B$ the triple product gives

$$(\mathbf{u}_1 \times \mathbf{u}_2) \cdot \mathbf{u}_3 = \frac{\sqrt{3}}{2} a^2 \sum x_i z(\mathbf{R}_B + \boldsymbol{d}_i). \tag{7.9}$$

Thus $e(\mathbf{R}_B)$ is a measure of the degree to which the three vertices and the pivot point of the specified tri-bond deviate from being coplanar. The physical nature of the distortion depends on the implementation of the model. If the tri-bond is realized as a triangular elastic sheet pinned at the pivot point, for example, $e \neq 0$ requires some bending of the sheet simple stretching of a spring attached to a rigid frame joining the three masses.

To lowest order in the displacements, the energy associated with a tri-bond must be quadratic in $e(\mathbf{R}_B)$, giving a total elastic energy

$$U = \frac{1}{2} k \sum_B e^2(\mathbf{R}_B), \tag{7.10}$$

where the sum is over all sites $\mathbf{R}_B$ in the B-sublattice. This energy has exactly the same form as that of a lattice of harmonic springs where the sum is over bonds and e is the elongation of a bond. Following this analogy, we call $e(\mathbf{R}_B)$ the *stretch* of the tri-bond at $\mathbf{R}_B$. Of course, with the aid of Eq. (7.8) we can express U as a function of the displacements $z(\mathbf{R}_A)$ instead of stretches $e(\mathbf{R}_B)$.

Given U, we can now construct expressions for the N_B tri-bond *tensions* $t(\mathbf{R}_B)$ conjugate to stretches of the tri-bonds and the N site forces $f(\mathbf{R}_A)$ conjugate to vertical displacements of the masses. As in the case of harmonic springs, $t(R_B)$ is simply the derivative of the energy with respect to $e(\mathbf{R}_B)$ and $f(\mathbf{R}_A)$ is the derivative of the energy with respect to the dynamical variable $z(\mathbf{R}_A)$:

$$t(\mathbf{R}_B) = \frac{\partial U}{\partial e(\mathbf{R}_B)} = k\, e(\mathbf{R}_B) \tag{7.11}$$

$$f(\mathbf{R}_A) = \frac{\partial U}{\partial z(\mathbf{R}_A)} = \sum_i x_i\, t(\mathbf{R}_A - \boldsymbol{d}_i) \tag{7.12}$$

which may be written in terms of the displacements as

$$t(\mathbf{R}_B) = k \sum_i x_i\, z(\mathbf{R}_B + \boldsymbol{d}_i) \tag{7.13}$$

$$f(\mathbf{R}_A) = k \sum_{i,j} x_i\, x_j\, z(\mathbf{R}_A - \boldsymbol{d}_i + \boldsymbol{d}_j). \tag{7.14}$$

The tension t is one that induces "stretching" of the tri-bond in a manner exactly analogous to the tension in a spring bond inducing stretching of the spring, and the force $f(\mathbf{R}_A)$ is a linear combination of the tension of bonds with endpoints sharing R_A, as is the case in systems of harmonic springs.

Introducing the N-dimensional vectors $\boldsymbol{z}$ and $\mathbf{f}$ of site-displacements and forces and the N_B dimensional vectors of $\mathbf{e}$ and $\boldsymbol{t}$ of stretches and tensions, we can write Eqs. (7.8), (7.11), and (7.12) as

$$\mathbf{e} = C\boldsymbol{z}; \qquad \boldsymbol{t} = k\mathbf{e}; \qquad \mathbf{f} = Q\boldsymbol{t}, \tag{7.15}$$

where C is the compatibility matrix with components

$$C(\mathbf{R}_B, \mathbf{R}_A) = \sum_i x_i \delta_{\mathbf{R}_B + \boldsymbol{d}_i, \mathbf{R}_A}, \tag{7.16}$$

and Q is the equilibrium matrix with components

$$Q(\mathbf{R}_A, \mathbf{R}_B) = \sum_i x_i \delta_{\mathbf{R}_A - \boldsymbol{d}_i, \mathbf{R}_B}. \tag{7.17}$$

$Q = C^T$ as required. In Fourier space,

$$e(\mathbf{q}) = C(\mathbf{q}) z(\mathbf{q}); \qquad f(\mathbf{q}) = Q(\mathbf{q}) t(\mathbf{q}), \tag{7.18}$$

where $C(\mathbf{q})$ and $Q(\mathbf{q})$ in this case are 1×1 matrices with

$$C(\mathbf{q}) = \sum_i x_i e^{i\mathbf{q}\cdot\boldsymbol{d}_i} = Q^*(\mathbf{q}). \tag{7.19}$$

As in the case of central-force springs, the null space of C consists of zero modes and that of Q of SSSs. The global and wave-number specific Maxwell-Calladine index theorems follow immediately:

$$N_0 - S = N - N_B \tag{7.20}$$

and

$$n_0(\mathbf{q}) - s(\mathbf{q}) = n - n_B, \tag{7.21}$$

where N_0 and S are, respectively, the total number of zero modes and the total number of SSSs, $n_0(\mathbf{q})$ and $s(\mathbf{q})$ are the numbers of zero modes and states of self stress at wavenumber $\mathbf{q}$, and n and n_B are the number of sites (1 under PBC) and number of tri-bonds (1 under PBC) per unit cell.

The energy can be written in various ways in terms of these variables:

$$E = \frac{k}{2N}\sum_{\mathbf{q}} |e(\mathbf{q})|^2 \tag{7.22}$$

$$= \frac{1}{2N}\sum_{\mathbf{q}} z(-\mathbf{q})D(\mathbf{q})z(\mathbf{q}) \tag{7.23}$$

$$= \frac{1}{2kN}\sum_{\mathbf{q}} |t(\mathbf{q})|^2, \tag{7.24}$$

where $D(\mathbf{q}) = k|C(\mathbf{q})|^2$ is the (one-dimensional) dynamical matrix. For the system with PBCs, the corresponding quantum Hamiltonian is block diagonal with 2×2 blocks of the form

$$H(\mathbf{q}) = \omega_0 \begin{pmatrix} 0 & C^*(\mathbf{q}) \\ C(\mathbf{q}) & 0 \end{pmatrix}, \tag{7.25}$$

where we define the normal mode frequency scale $\omega_0 = \sqrt{k}$. The square of this Hamiltonian is diagonal with lower entry kCC^* and upper entry $kC^*C = D$ (which are identical as C is one-dimensional). The eigenvalues of $H(\mathbf{q})$, given by $\pm\omega(\mathbf{q})$, are simply the two square roots of D and thus specify the normal mode dispersion $\omega(\mathbf{q})$, with $C(0) = 1$ implying $\omega_0 = \omega(\mathbf{q} = 0)$.

If we identify the bond hopping amplitudes $t_i = \omega_0 x_i$, then $H(\mathbf{q})$ is formally identical to the Hamiltonian of the nearest neighbor tight binding model of graphene . Equivalently, the constraint $\sum x_i = 1$ corresponds to setting $\omega_0 = \sum_i t_i$.

B. Weyl Points and Phase Diagram

The spectrum and topological properties of mechanical graphene depend on the location of the pivot point in the tri-bond. The features of the different models can thus be represented on a ternary phase diagram in which each point (x_1, x_2, x_3) corresponds precisely to

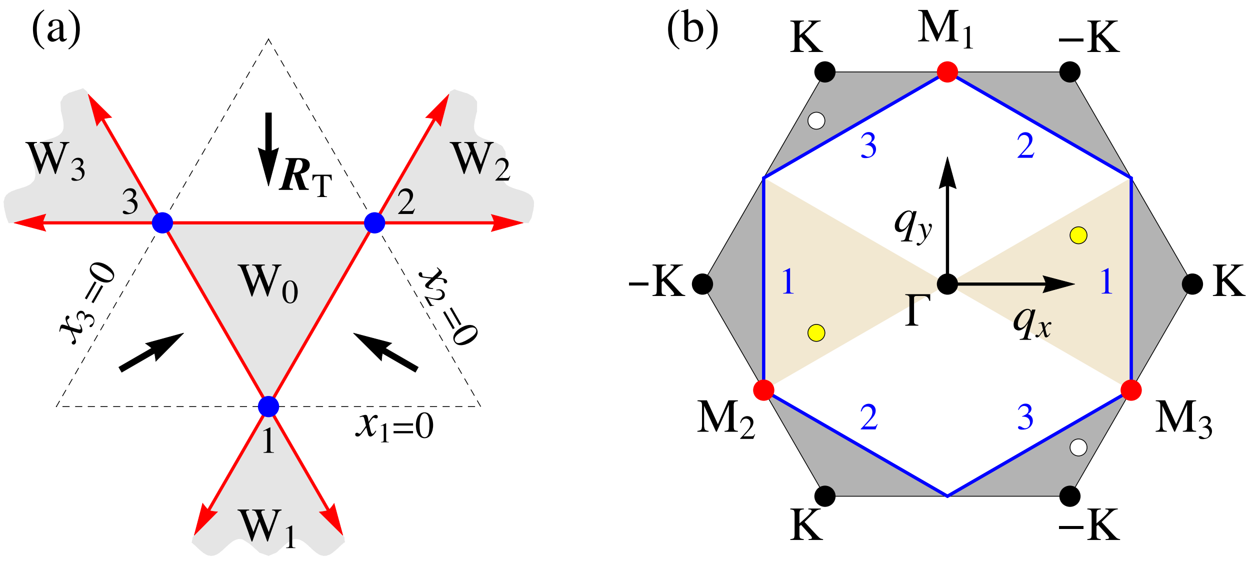

FIG. 19. (a) Ternary phase diagram of strained graphene. The dashed triangle marks the boundary of the region in which all x_i's are positive. In each region marked W_i, there are two Weyl points in the Brillouin zone. In the other regions, the bands are characterized by nonzero winding numbers when traversed in the directions indicated by arrows. (b) The Brillouin zone with high symmetry points marked, including $\mathbf{K} = (4\pi/3a, 0)$ (and equivalent points) and $\mathbf{M}_1 = (0, 2\pi/\sqrt{3}a)$. Dark gray (light tan) shaded regions indicate possible locations of Weyl points corresponding to region W_0 (W_1), with white (yellow) disks showing generic possible arrangements. At each blue point i $(= 1, 2, 3)$ in (a), there are zero modes along the pair of blue lines marked i in (b). Along each red line in (a), there is a red point in (b) containing degenerate Weyl points.

the placement of the pivot point. Unlike a typical ternary phase diagram, however, negative values of x_i (corresponding to pivot points outside the triangle) are allowed here.

In this section, we will derive the phase diagram shown in Fig. 19(a), in which there are three gapped regions with different topological polarizations $\mathbf{R}_T$ and four regions, $\mathrm{W}_{0,1,2,3}$, with Weyl points. The point $x = (1/3, 1/3, 1/3)$ corresponds to undistorted graphene. Other points correspond to strained graphene, though the regions outside W_0 correspond to degrees of strain that are probably too large to be physically realizable.

Weyl points arise when $C(\mathbf{q}) = 0$, which generically occurs for pairs of points $\pm\mathbf{q}^*$, where $\mathbf{q}^*$ is a solution of

$$C(\mathbf{q}^*) = x_1 e^{i\mathbf{q}^*\cdot\boldsymbol{d}_1} + x_2 e^{i\mathbf{q}^*\cdot\boldsymbol{d}_2} + x_3 e^{i\mathbf{q}^*\cdot\boldsymbol{d}_3} = 0. \tag{7.26}$$

When $x = (1/3, 1/3, 1/3)$ (at the middle of W_0 in Fig. 19(a)) Eq. (7.26) is satisfied at the

±K points $\mathbf{q}^* = \pm\mathbf{q}_{\rm K}$, where

$$\mathbf{q}_{\rm K} = \frac{4\pi}{3a}\hat{x} \quad \Rightarrow \quad e^{i\mathbf{q}_{\rm K}\cdot\boldsymbol{d}_j} = e^{2\pi i(j-1)/3}. \tag{7.27}$$

This corresponds to the well known Weyl point at the Brillouin zone corner in unstrained graphene. In Fig. 20(a) we show the displacements of one of the zero frequency modes at $\mathbf{q}_{\rm K}$. It is straightforward to see in Fig. 20(a) that this is indeed a "floppy mode" in which, to linear order, each tri-bond undergoes a rigid rotation about its pivot point and hence is not stretched.

Because the phase of $C(\mathbf{q})$ advances by 2π as $\mathbf{q}$ wraps around $\mathbf{q}^*$, the Weyl points are locally protected and cannot be removed by a smooth deformation. Therefore, there must be a Weyl phase in a finite region around $(1/3, 1/3, 1/3)$. However, it is also clear from (7.26) that for $x = (1, 0, 0)$, $(0, 1, 0)$ or $(0, 0, 1)$ there are no solutions to $C(\mathbf{q}^*) = 0$. Thus, there must be a gapped phase in the vicinity of the three corners of the dashed triangle in Fig. 19(a).

To determine the phase boundaries, we note that Weyl points can only only disappear if they meet, which must occur at a time-reversal-invariant point $\mathbf{q}^* = -\mathbf{q}^* + \mathbf{G}$, where $\mathbf{G}$ is a reciprocal lattice vector. $\mathbf{q}^* = 0$ is ruled out for finite x because $C(0) = x_1 + x_2 + x_3 = 1$, so this must occur at one of the three M points

$$\mathbf{q}_{{\rm M}j} = \frac{2\pi}{\sqrt{3}a}\hat{\boldsymbol{d}}_j, \tag{7.28}$$

which satisfy

$$\mathbf{q}_{{\rm M}j} \cdot \boldsymbol{d}_k = \begin{cases} 2\pi/3 & j = k \\ -\pi/3 & j \neq k \end{cases}. \tag{7.29}$$

Then Eq. (7.26) requires

$$x_k - x_{k-1} - x_{k+1} = 0 \tag{7.30}$$

where the subscript is defined cyclically. Together with $\sum x_i = 1$, this implies $x_k = 1/2$ and $x_{k-1} + x_{k+1} = 1/2$, which define the three red lines bounding the triangle inscribed in the dashed region of Fig. 19(a). The Weyl phase in the vicinity of $x = (1/3, 1/3, 1/3)$ thus corresponds to the region W_0. On the boundary of W_0 the Weyl points meet and annihilate.

The points outside the dashed triangle of Fig. 19(a) have the pivot outside the tri-bond and have one or two of the x_i negative. This corresponds in the graphene model to having bond(s) with a negative hopping amplitude. Systems with negative hopping amplitudes

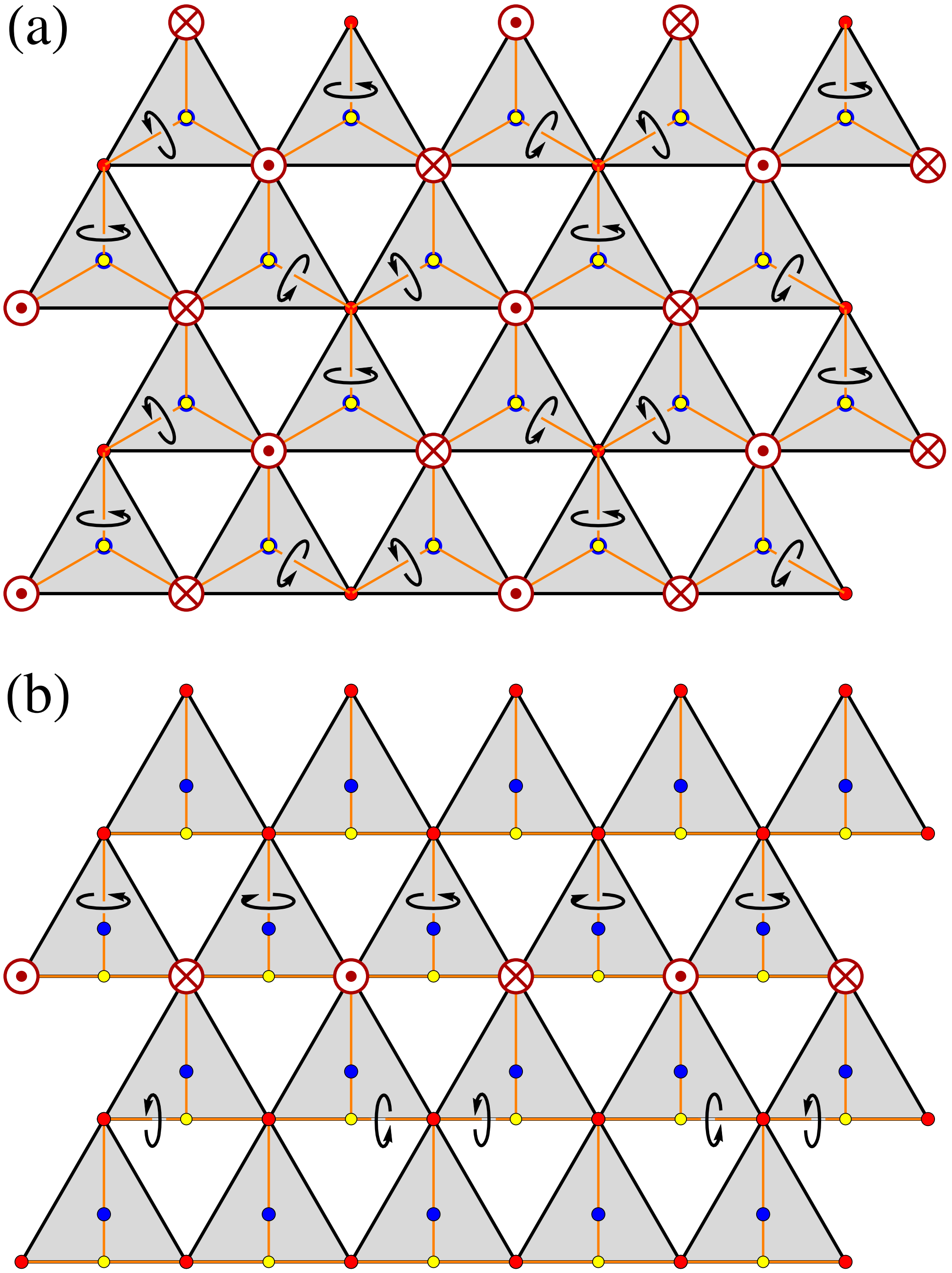

FIG. 20. (a) A Weyl mode for $x = (1/3, 1/3, 1/3)$, corresponding to unstrained graphene. The pivot is at the centroid of the tri-bond. (b) A zero mode for $x = (0, 1/2, 1/2)$. The mode is confined to a single line. The pivot point is at the midpoint of the bottom edge, and each tri-bond rotates rigidly about its pivot so that vertices move in and out of the plane as indicated.

are closely related to systems with positive hopping amplitudes. The sign of the hopping amplitude on one of the three bonds (say along $\mathbf{d}_1$) can be changed by a non-uniform gauge transformation that changes the signs of all sites on every other horizontal (zig-zag) line of bonds on the honeycomb lattice. This transformation takes bond hopping amplitudes $(t_1, t_2, t_3) \to (-t_1, t_2, t_3)$, which in our mechanical model takes $x = (x_1, x_2, x_3) \to x' = (-x_1, x_2, x_3)/(x_2 + x_3 - x_1)$. This gauge transformation does not change the normal mode frequencies except for an overall constant factor due to the relation between x_i and t_i. However, since the gauge transformation is at a nonzero wavevector $\mathbf{q}_{\mathrm{M1}}$, it leads to a shift in the wavevector of the normal modes and hence a transformation of the dispersion relation:

$$\omega_{x'}(\mathbf{q}) = (x_2 + x_3 - x_1)^{-1}\omega_x(\mathbf{q} + \mathbf{q}_{\mathrm{M1}}). \tag{7.31}$$

This transformation maps $x = (1/3, 1/3, 1/3)$ to $x' = (-1, 1, 1)$, so the normal mode spectra at these two pivot point locations are related by Eq. (7.31). In particular, for x' there are Weyl points at $\mathbf{q}_{\mathrm{K}} + \mathbf{q}_{\mathrm{M1}}$. Indeed, Eq. (7.26) is satisfied for $\mathbf{q}^* = \pm\mathbf{q}_{\mathrm{L}}$, where

$$\mathbf{q}_{\mathrm{L}} = \frac{2\pi}{3a}\hat{x} \quad \Rightarrow \quad e^{i\mathbf{q}_{\mathrm{L}}\cdot\boldsymbol{d}_{(1,2,3)}} = (e^0, e^{\pi i/3}, e^{-\pi i/3}). \tag{7.32}$$

It can be checked that $\mathbf{q}_{\mathrm{L}} = -\mathbf{q}_{\mathrm{K}} + \mathbf{q}_{\mathrm{M1}}$ up to a reciprocal lattice vector. More generally, the Weyl phase W_0 maps to the region W_1 in Fig. 19(a). Similar transformations identify the Weyl phases W_2 and W_3, whose boundaries are again given by the red lines defined by Eq. (7.30).

When x is in W_0 in Fig. 19(a), the Weyl points are at $\pm\mathbf{q}^*$, which reside in the dark gray regions of Fig. 19(b). When x is in W_1, the Weyl points are at $\pm\mathbf{q}^*$ residing in the light tan regions of Fig. 19(b), and there are symmetry related regions corresponding to W_2 and W_3. When a path through W_0 is traversed, beginning on one edge and ending another, a pair of Weyl points created at M_j pass through the diametrically opposite dark gray regions of Fig. 19(b) and annihilate at $\mathrm{M}_{j\pm1}$. Similarly, for a path that begins on right boundary of W_1, passes through W_1, and terminates on the left boundary, the Weyl points are born at $\pm\mathrm{M}_2$, pass through the opposite tan regions of Fig. 19(b), and annihilate at $\pm\mathrm{M}_3$. For $x = (-\alpha, (\alpha + 1)/2, (\alpha + 1)/2)$ with $\alpha \gg 1$, Weyl points occur at $\mathbf{q}^* \approx \pm(2\sqrt{2/\alpha}/a)\hat{x}$, converging to the Γ point as $\alpha \to \infty$.

Outside the W_n regions there is a gap everywhere in the Brillouin zone. There are three disconnected phases that are topologically distinct. The topological polarization can be most easily evaluated at the three simple points (indexed by $j = 1, 2, 3$) $x_i = \delta_{ij}$. Then,

$$C(\mathbf{q}) = e^{i\mathbf{q}\cdot\boldsymbol{d}_j}. \tag{7.33}$$

The topological polarization $\mathbf{R}_T$ is determined by the winding numbers n_i of this phase over the independent cycles of the Brillouin zone:

$$n_i = -\frac{1}{2\pi i}\oint_{C_i} C^{-1} dC = -\frac{1}{2\pi}\boldsymbol{b}_i \cdot \boldsymbol{d}_j \tag{7.34}$$

where C_i is the cycle along reciprocal lattice generator $\boldsymbol{b}_i$, which satisfies $\boldsymbol{b}_i \cdot \boldsymbol{a}_j = 2\pi\delta_{ij}$ for Bravais lattice generators $\boldsymbol{a}_j$. (Note the minus sign in this equation, which appears because it is defined as an integral over $C(\mathbf{q})$ rather than $Q(\mathbf{q})$ as in .) Writing

$$\mathbf{R}_T = n_1\boldsymbol{a}_1 + n_2\boldsymbol{a}_2 \tag{7.35}$$

then gives

$$\mathbf{R}_T = -\boldsymbol{d}_j, \tag{7.36}$$

which follows from the "completeness" relation $\sum_{i=1}^{2} \boldsymbol{a}_i\boldsymbol{b}_i = 2\pi I$, where I is the unit matrix. The value of $\mathbf{R}_T$ depends on the real-space positions assigned to the A and B lattice sites, i.e., on our gauge choice. In our current symmetric choice, in which the B sites do not sit at a center of inversion, $\mathbf{R}_T$ is not a lattice vector, but the *differences* between of $\mathbf{R}_T$'s in different phases are. Arrows indicating $\mathbf{R}_T$ are indicated in Fig. 19(a). (In the gauge where the origin lies at an A site, we subtract a particular $\boldsymbol{d}_k$ from each $\boldsymbol{d}_j$ in Eq. (7.33), and the n_i are all 0 or ± 1.)

Finally, we note that the line in the phase diagram corresponding to $x_1 = 0$ (where the pivot point is along the bottom edge of the tri-bond) corresponds to a one dimensional limit, in which the system consists of decoupled horizontal lines that are similar to the SSH model. In this case there is a direct transition between topologically distinct gapped phases, which occurs at the blue point $x = (0, 1/2, 1/2)$. Here

$$C(\mathbf{q}) = \cos(q_x a/2)e^{-iq_y a/(2\sqrt{3})}, \tag{7.37}$$

so that there is a *line* of zero modes at $q_x = \pm\pi/a$ along the vertical line that connects M_2 and M_3, indicated by a blue line in Fig. 19(b). This situation is analogous to that in critical kagome lattices when there are parallel straight lines of bonds . The zero modes are easy to visualize: as we have discussed, rotation of a tri-bond about any axis passing through its pivot point produces no stretch and costs no energy. Consider a horizontal line of edges containing the $\boldsymbol{d}_2$ and $\boldsymbol{d}_3$ vertices of the row of tri-bonds above it and the $\boldsymbol{d}_1$ vertex of the row of tri-bonds below it as shown in Fig. 20(b). Rotating neighboring tri-bonds in the upper row by $\delta\theta$ in opposite directions about the axis passing through the pivot point and $\boldsymbol{d}_1$ (the top vertex) while rotating neighboring tri-bonds in the lower row in opposite directions by $\delta\theta/\sqrt{3}$ about the axis along their bottom edges produces a zero mode. This operation only affects the given rows, and there is a zero mode for each line of bonds.

Associated with each zero mode, there must be a state of self stress. Alternating equal-amplitude stresses on tri-bonds along any row produces the desired zero-force state. In the case with $x_1 = 0$ and $x_2 = x_3 = 1/2$, the stress tends to bend the tri-bonds symmetrically either upward or downward about a line passing through the pivot point and vertex 1. Alternation of the sign of the stresses causes vertices 2 and 3 to experience equal and opposite forces from the two tri-bonds each shares along the x axis. When $x_2 \neq x_3$, neighboring rows are still decoupled, and each is equivalent to the SSH model, whose critical point occurs when $x_2 = x_3$. Thus the lines defined by $x_i = 0$ for some i, which include the perimeter of the region where all x_i are positive, correspond to the 1D limit.

C. Edge States

Strips with periodic boundary conditions in one direction or samples with free sides on all boundaries can be produced by removing lines of tri-bonds from the system under full periodic boundary conditions. Each line of cut tri-bonds creates two free edges. Since the number of sites and tri-bonds are equal under periodic boundary conditions, the index theorem reduces to

$$N_0 - S = \Delta N_B \tag{7.38}$$

where ΔN_B is the total number of tri-bonds cut to produce the free edges. A similar equation applies to each wavenumber q along the cut producing a strip:

$$n_0(q) - s(q) = \Delta n_B, \tag{7.39}$$

where Δn_B is the number of bonds cut per unit cell of one of the exposed edges. How zero modes are distributed on the free edges depends on the topological polarization $\mathbf{R}_T$ and a local surface polarization $\mathbf{R}_L$ according to the same formula derived for central-force

Maxwell lattices. The number of zero modes per edge unit cell (or equivalently per edge wavenumber q) for a given edge corresponding to a lattice "plane" indexed by the reciprocal lattice vector $\mathbf{G}$ pointing along the edge's *outer normal* is

$$n_0 = (\mathbf{R}_T + \mathbf{R}_L) \cdot \mathbf{G}/(2\pi). \tag{7.40}$$

The local polarization $\mathbf{R}_L$ is simply the electric polarization at the given edge that arises from assigning a charge $+1$ to sites on the A-sublattice and a charge -1 to sites on the B sublattice. Of course only components of $\mathbf{R}_L$ parallel to $\mathbf{G}$ contribute to n_0 so we are free to add arbitrary components to $\mathbf{R}_L$ parallel to the edge .

It is instructive to look at a couple of examples. Consider the strip with edges parallel to the x-axis as shown in Fig. 20(b). To produce this strip, one tri-bond per surface unit cell had to be removed, so there is a total of one zero mode per wavenumber on the two exposed edges. The local polarization $\mathbf{R}_L^L$ on the lower edge with outer surface normal, $\mathbf{G} = -4\pi/\sqrt{3}a\hat{y}$, is equally well represented by $-\boldsymbol{d}_1/2$, $\boldsymbol{d}_2$, or $\boldsymbol{d}_3$, giving a local contribution to the number of edge zero modes of 1/3. On the upper surface $\mathbf{R}_L^U = +\boldsymbol{d}_1$, for a contribution of 2/3 to edge-mode count. The topological count for the bottom surface is respectively 2/3, $-1/3$, and $-1/3$ for $\mathbf{R}_T$ equal to $-\boldsymbol{d}_1$, $-\boldsymbol{d}_2$, and $-\boldsymbol{d}_3$ for a total of one zero mode on the bottom surface and none on the top surface for $\mathbf{R}_T = -\boldsymbol{d}_1$ and no zero mode on the bottom and one the top surface for $\mathbf{R}_T = -\boldsymbol{d}_2, -\boldsymbol{d}_3$. A similar analysis for a strip parallel to the y-axis yields for the number of zero modes on the left and right surfaces $(n_0^R, n_0^L) = (1,1)$, $(0,2)$, and $(2,0)$ for $\mathbf{R}_T$ equal to $-\boldsymbol{d}_1$, $-\boldsymbol{d}_2$, and $-\boldsymbol{d}_3$, respectively. When there are Weyl points, zero modes shift from one side of a strip to the other at edge wavenumbers equal to the projections of the wavenumber of the Weyl points onto the edge.

Insight into Eq. (7.40) can be gained by considering what happens to C when the sites and tri-bonds are indexed at different positions (without changing the lattice itself). Let

$$\mathbf{R}'_A = \mathbf{R}_A + \Delta\mathbf{R}_A \quad \text{and} \quad \mathbf{R}'_B = \mathbf{R}_B + \Delta\mathbf{R}_B, \tag{7.41}$$

and define the "gauge-transformed" compatibility matrix,

$$C'(\mathbf{R}'_A, \mathbf{R}'_B) = C(\mathbf{R}'_A - \Delta\mathbf{R}_A, \mathbf{R}'_B - \Delta\mathbf{R}_B). \tag{7.42}$$

Then

$$C'(\mathbf{q}) = e^{-i\mathbf{q}\cdot(\Delta\mathbf{R}_A - \Delta\mathbf{R}_B)} C(\mathbf{q}) = |C(\mathbf{q})|\, e^{-i\mathbf{q}\cdot(\Delta\mathbf{R}_A - \Delta\mathbf{R}_B + \mathbf{R}_T)}. \tag{7.43}$$

Thus if we chose $\Delta\mathbf{R}_A - \Delta\mathbf{R}_B = \mathbf{R}_L$, we find that the total polarization of $C'(\mathbf{q})$ is $\mathbf{R}' = \mathbf{R}_L + \mathbf{R}_T$. Let $\mathbf{q} = (q_\perp, q_\|)$, where $q_\perp$ and $q_\|$ are, respectively, the components of $\mathbf{q}$ perpendicular (positive toward the sample interior) and parallel to the lattice plane in question, and define $\eta = \exp(iq_\perp a_\perp)$, where $a_\perp$ is the depth of the surface unit cell, and $0 < q_\perp \le |\mathbf{G}|$, where $\mathbf{G}$ is the inner normal reciprocal lattice vector associated with the lattice plane. $C'(\eta, q_\|)$ contains only positive powers of η, and thus no poles in η, and as a result, the integral

$$n_0(\mathbf{G}) = \frac{1}{2\pi i}\oint d\eta \frac{d}{d\eta}\ln C'(\eta, q_\|) = \frac{\mathbf{G}\cdot(\mathbf{R}_L + \mathbf{R}_T)}{2\pi} \tag{7.44}$$

counts the number of zero modes at the surface determined by $\mathbf{G}$. As particular examples, consider the bottom and left edges in Fig. 18. In the first case, $\mathbf{R}_L = -\boldsymbol{d}_1/2$ and

$$C'(\eta, q_x) = x_1\eta + x_2 e^{-iq_x a/2} + x_3 e^{iq_x a/2}, \tag{7.45}$$

where $\eta = \exp(iq_y\sqrt{3}\,a/2)$, has at most one zero and no poles, in agreement with our result that the top and bottom surfaces can have either one zero mode or none. In the second case, $\mathbf{R}_L = \boldsymbol{d}_2$, and

$$C'(\eta, q_x) = x_3\eta^2 + x_1\eta + x_2 e^{iq_y\sqrt{3}\,a/2}, \tag{7.46}$$

where $\eta = \exp(iq_x a/2)$. Again, there are no poles, but the highest power of η is 2, and according to Eq. (7.44), there can be 0, 1, or 2 zero modes in agreement with our previous results.

When there are Weyl modes, the number of zero modes on a free edge of a strip will change when $q_\|$ passes through the projection of a Weyl point onto that edge . The total number of zero modes does not change at this transition, so there must be a change of the opposite sign in the number of zero modes on the opposite edge. In other words, zero modes move from one side of the sample to the opposite at a projection of a Weyl point. A similar phenomenon occurs at domain walls in systems under periodic boundary conditions, in which the number of zero modes equals the number of states of self-stress and is given by

$$\nu_T = \mathbf{G}\cdot(\mathbf{R}_T^1 - \mathbf{R}_T^2)/2\pi, \tag{7.47}$$

where ν_T is equal to the number of zero modes per wavenumber if it is positive and minus the number of states of self stress if it is negative. Thus a change in the number of zero modes on a zero-mode domain wall, which occurs at $q_\|$ equal to the projected Weyl wavenumber, must be accompanied by an equal change in the number of Weyl states of self-stress on a self-stress domain wall.

VIII. TOPOLOGICAL PHONON LATTICES

References:

Kane, C. L., and T. C. Lubensky. ”Topological Boundary Modes in Isostatic Lattices.” Nature Physics 10, no. 1 (Jan 2014): 39-45.

Stenull, O., C. L. Kane, and T. C. Lubensky. ”Topological Phonons and Weyl Lines in Three Dimensions.” Physical Review Letters 117, no. 6 (Aug 2016): 068001.

Mao, X. M., and T. C. Lubensky. ”Maxwell Lattices and Topological Mechanics.” In Annual Review of Condensed Matter Physics, Vol 9, edited by S. Sachdev and M. C. Marchetti. Annual Review of Condensed Matter Physics, 413-33, 2018.

We have seen that unlike electron systems, the strips of the fully gapped Maxwell lattice we are considering have a number of edge states equal to the number of bonds that are cut to produce the strip from the lattice under periodic boundary conditions. We have also seen in a one-dimensional example without acoustic phonons that different topological states, characterized by different winding numbers of the compatibility matrix, can be constructed and that the two topological lattices have zero edge modes on different sides of the lattice. The question then is, can we construct lattices that both obey the Maxwell count of zero edge modes and that have topological characterizations that upon change can move zero modes from one free surface to another. The answer is of course yes. Fig. (21) shows three lattices constructed from the kagome lattice. The center lattice (b) has one set of straight segments parallel to the x-axis. These give rise to states of self-stress and associated bulk zero modes along $q_x = 0$ in the Brillouin zone. This lattice is the analog of the state with $\bar{\theta} = 0$ in the one-dimensional example. Figure (a) shows the three-fold symmetric twisted kagome lattice and (c) shows a new lattice that has a different topological characterization from the twisted kagome lattice. Both lattices (a) and (c) have a fully gapped spectrum, though lattice (c) has phonon modes with frequency proportional along certain directions to q^2 rather than q, and both can be obtained from lattice (b) by continuous distortion. Thus (a) and (c) are the analogs of the $\theta = \pm\bar{\theta}$. They have gaps that continuously approach zero as lattice (b) is approached.

1. Let $\nu^S = N_0 - N_S$ be the number of zero modes minus the number of states of self stress in a subsystem, which could include a free surface or a buried interface. If the bulk

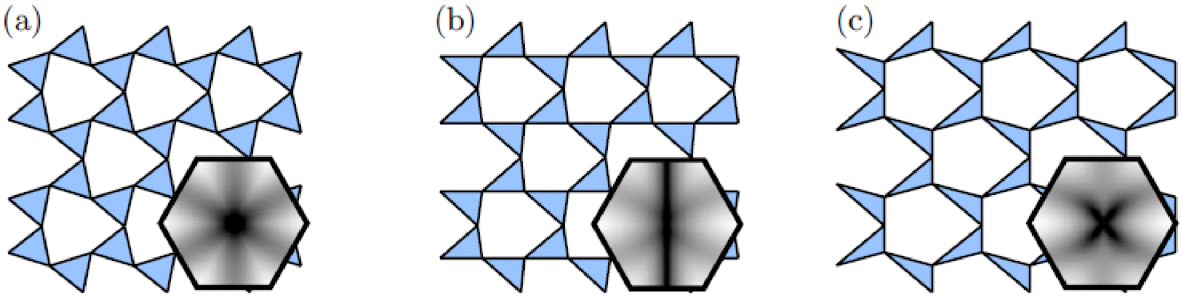

FIG. 21. (a) Non-topological, (b) critical, and (c) topological kagome lattices.

modes are gapped, then the zero modes are necessarily at free or buried surfaces. It a particular surface has zero modes, it will not have states of self stress and vice-versa. ν_L can be decomposed into a local part and ν_L^S and a topological part ν_T^S:

$$\nu^S = \nu_L^S + \nu_T^S \tag{8.1}$$

To evaluate these quantities, it is useful to introduce a kind of dipole moment. Associate with each site a charge 2 (charge d in d dimensions) and with each bond a charge -1. Because there are three sites and six bonds in each unit cell, the total charge of each unit cell is zero. There can, however, be a nonzero dipole moment, depending both on the shape of the unit cell and on the gauge (recall - assignment of positions to bonds and sites).

2. Symmetric unit cells [Fig. (22)] in the kagome lattice have a dipole moment of zero. The dipole moment is

$$\mathbf{R}_L = d \sum_{\text{sites}\,\mu} \tilde{\vec{r}}_\mu - \sum_{\text{bonds}\,\beta} \tilde{\vec{r}}_\beta. \tag{8.2}$$

Because the dipole moment of the symmetric cell is zero, the moments of surface compatible cells can be calculated by calculating the change in moment brought about by moving bonds an sites from the symmetric cell to the surface cell yielding displacements $\Delta\tilde{\vec{r}}_\mu$ and $\Delta\tilde{\vec{r}}_\beta$ so that

$$\mathbf{R}_L = d \sum_{\text{sites}\,\mu} \Delta\tilde{\vec{r}}_\mu - \sum_{\text{bonds}\,\beta} \Delta\tilde{\vec{r}}_\beta. \tag{8.3}$$

Note, because the shifts $\Delta\tilde{\vec{r}}_\mu$ and $\Delta\tilde{\vec{r}}_\beta$ are necessarily multiples of lattice vectors $\mathbf{R}_L$ is a lattice vector. Examples of shifted cells are shown in the figure. The local count

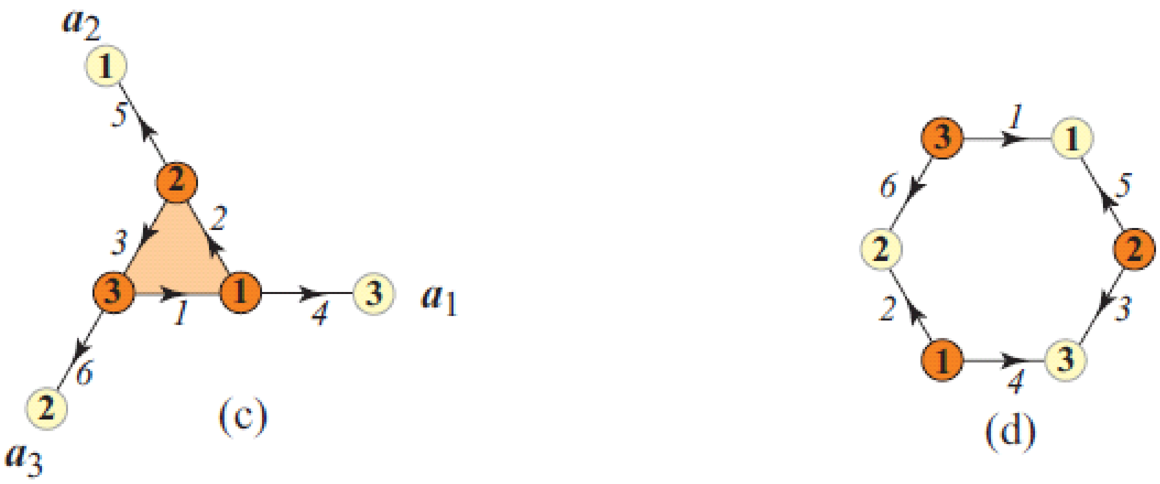

FIG. 22. Two symmetric cells with dipole moment equal to zero.

per site is

$$\tilde{\nu}_L \equiv \nu_L^S / N_{\text{cell}} = \mathbf{G} \cdot \mathbf{R}_L / 2\pi, \tag{8.4}$$

where $\mathbf{G}$ is the reciprocal lattice vector associated with the surface cut point away from the surface [Fig. (23)].

3. The topological count is similar to the index for the one-dimensional system. It too can be expressed in terms of a lattice vector $\mathbf{R}_T$, which can be viewed as a topological polarization.

$$\tilde{\nu}_T^S = \nu^S / N_{\text{cell}} = \mathbf{G} \cdot \mathbf{R}_T / (2\pi), \tag{8.5}$$

where N_{cell} is the number of surface unit cells and $\mathbf{R}_T$, a generalization of the one-dimensional winding number, is a lattice vector

$$\mathbf{R}_T = \sum_i n_i \boldsymbol{a}_i, \tag{8.6}$$

where $\boldsymbol{a}_i$ are the primitive translation vectors and

$$n_i = \frac{1}{2\pi i} \oint_{C_i} d\mathbf{q} \cdot \text{Tr}[\mathbf{Q}(\mathbf{q})^{-1} \nabla_{\mathbf{q}} \mathbf{Q}(\mathbf{q})]. = \frac{1}{2\pi} \oint_{C_i} d\mathbf{q} \cdot \nabla_{\mathbf{q}} \phi(\mathbf{q}), \tag{8.7}$$

where $\phi(\mathbf{q})$ is the phase of $\det \mathbf{Q}(\mathbf{q})$ ($\mathbf{Q}(\mathbf{q}) = |\mathbf{Q}(\mathbf{q})|^{i\phi(\mathbf{q})}$). Here C_i is a cycle of the BZ connecting $\mathbf{q}$ and $\mathbf{q} + \boldsymbol{B}_i$, where $\boldsymbol{B}_i$ is a primitive reciprocal vector satisfying $\boldsymbol{a}_i \cdot \boldsymbol{B}_j = 2\pi\delta_{ij}$ ($\boldsymbol{B}_1 = -\mathbf{G}_2$ and $\boldsymbol{B}_2 = \mathbf{G}_1$. The n_i are winding numbers of the phase of $\det \mathbf{Q}(\mathbf{q})$ around the cycles of the BZ, where $\mathbf{Q}(\mathbf{q})$ is the equilibrium matrix in a

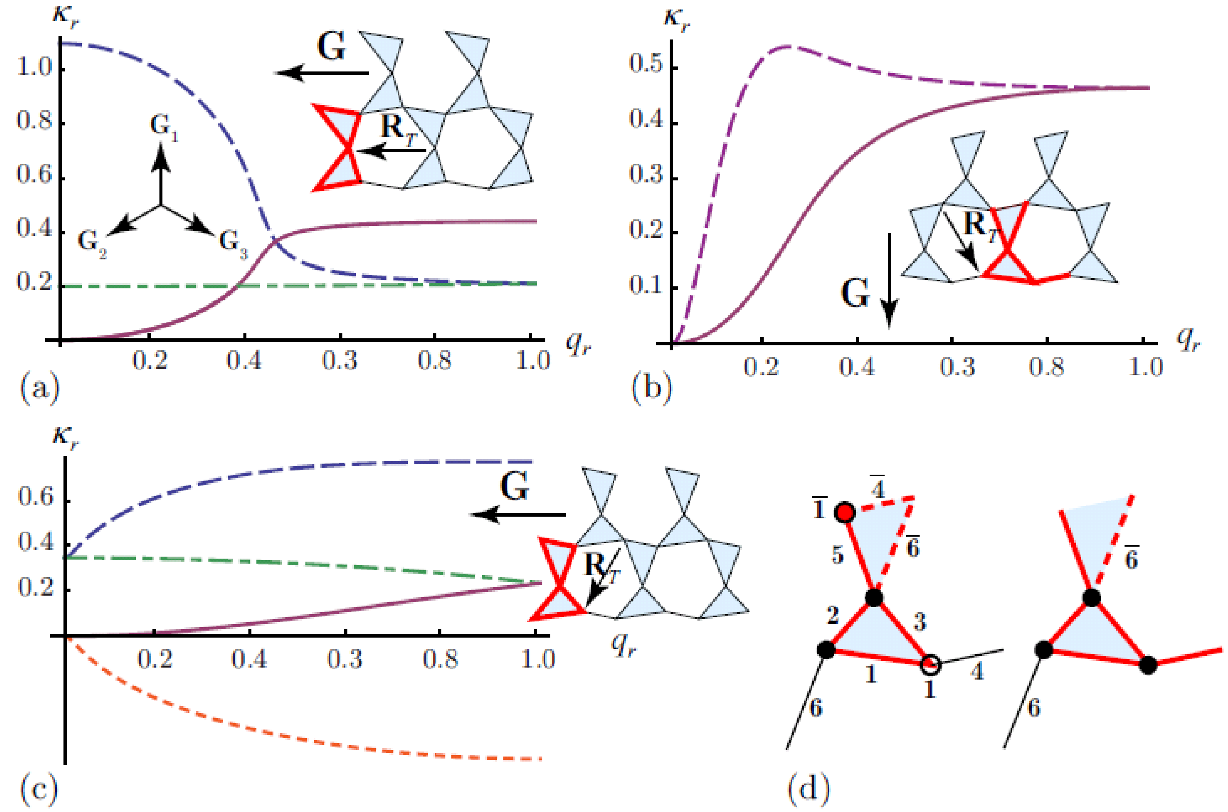

FIG. 23. Penetration depths for different orientations of $\mathbf{R}_T$ and lattices edges of a topological lattice. (a) Inverse penetrations depths, κ_r as a function of edge wavenumber q_r for an edge with four zero modes (the oppostie surface has zero). The solid line is doubly degenerate, and it is proportional to q_r^2 at small q_r. (b) And edge with two zero modes. (c) Lattice with three zero modes on the left edge and one on the right edge.

Bloch basis.

4. The derivation of theses results, which is fairly technical, provided in the supplementary material for the Nature Phys. article.

5. On domain walls [Fig. (24)], separating regions with different polarizations, the local count is zero because there are no broken bonds, and the total count is due only to the polarization charge.

$$\tilde{\nu}_T = \mathbf{G} \cdot (\mathbf{R}_T^1 - \mathbf{R}_T^2)/2\pi. \tag{8.8}$$

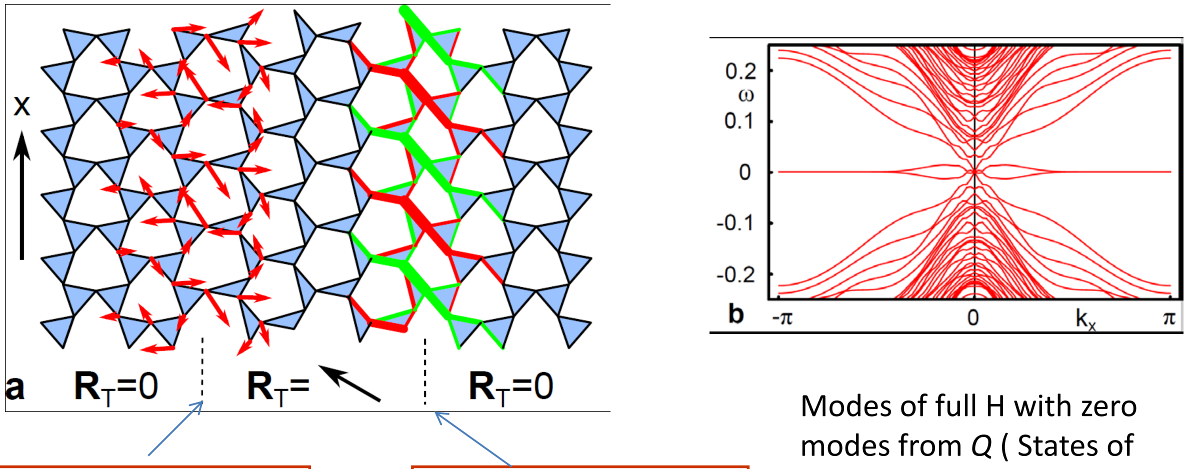

$$\nu_T = \frac{\mathbf{G}\cdot(\mathbf{R}_T^l - \mathbf{R}_T^r)}{2\pi} = 1$$

zero modes

$$\nu_T = \frac{\mathbf{G}\cdot(\mathbf{R}_T^l - \mathbf{R}_T^r)}{2\pi} = -1$$

States of Self Stres

Modes of full H with zero modes from *Q* (States of self stress) and form Q^T (zero modes)

FIG. 24. Zero-mode and state-of-self-stress domain walls.

If this is positive, there are zero modes. If it is negative, there are states of self stress. Under periodic boundary conditions, $N_0 = N_S$, and if there is a domain wall with N_0 zero modes, there must be one with $N_S = N_0$ states of self-stress. If there is a domain wall connecting two finite strips, the number of zero modes per cell must still equal the number of bonds that were cut. Thus for example, there could be one zero mode on the bottom surface, one zero mode at the domain wall, and no zero modes on the top surface.

6. Alternative domain wall count: There are cases (e.g., when there are Weyl mode (see later)) when it is not possible to cleanly define a polarization, but it is always possible to determine the number of zero modes for each free surface at each $\mathbf{q}$. From this information and the number of bonds per cell that have to be cut to break up the domain wall that joins two topologically distinct lattices, it is always possible to calculate the number of zero modes at the domain wall. Let n_{0R} and n_{0L} be the number of zero modes per unit cell (or equivalently per surface wavenumber) of the right and left free surfaces that are joined by n_B bonds per cell. There is a zero mode

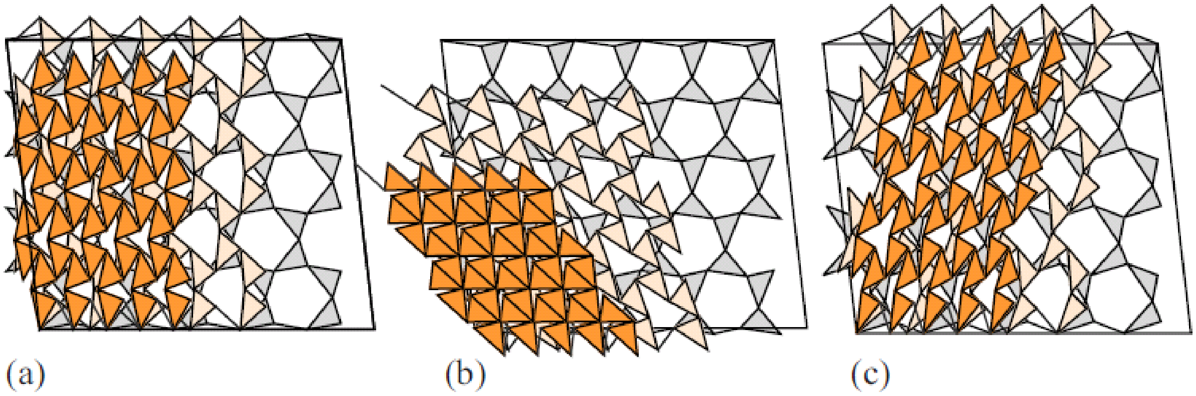

FIG. 25. Guest-Hutchinson modes for different lattices. (b) is auxetic but (a) and (c) are not.

at the domain wall whenever the zero modes of the free surfaces can be joined without stretching the added bonds creating the domain wall. There is a kind of compatibility matrix relating the stretches of the n_B bonds to the $n_{0R} + n_{0L}$ amplitudes of the surfaces modes on the two sides. The dimension of the null space of this matrix is the number of zero modes (per wavenumber) at the domain wall. Since there are no states of self-stress, the dimension of the range of this matrix is equal to n_B implying that the number of zero modes at the domain wall is

$$n_{0D} = n_{0R} + n_{0L} - n_B. \tag{8.9}$$

Thus in the example of Fig. 23, $n_{0L} = 2$, $n_{0R} = 1$, $n_B = 2$ and $n_{0D} = 2 + 1 - 2 = 1$. On the other hand if the lattice in fig. 23 (a) were joined with its mirror image, $n_{0R} = n_{0l} = 4$, $n_B = 4$ and $n_{0D} = 8 - 4 = 4$.

7. Elastic properties of topological Maxwell lattices: Each of fully gapped two-dimensional Maxwell lattice has one Guest mode. In the twisted kagome lattice, the mode is simply isotropic compression. It is more complicated in the family of distorted kagome lattices as shown in Fig. (25). Those with zero polarization generally have a negative and those with nonzero polarization have a positive Poisson ratio. See figure and Mathematic animation. The different in Guest modes lead to different long-wavelength phonon behavior with zero polarization having a linear dispersion and positive polarization having lines with quadratic dispersion.